PLK4 *trans*-autoactivation controls centriole biogenesis in space

Carla A.M. Lopes[1,7], Swadhin Chandra Jana[1,7], Inês Cunha-Ferreira[1,2,7], Sihem Zitouni[1,8], Inês Bento[1,3,8], Paulo Duarte[1], Samuel Gilberto[1,4], Francisco Freixo[1,6], Adán Guerrero[1,5], Maria Francia[1], Mariana Lince-Faria[1], Jorge Carneiro[1], Mónica Bettencourt-Dias[1,9]

[1] Instituto Gulbenkian de Ciência, Oeiras, Portugal

[2] Present address: Cell Biology, Faculty of Science, Utrecht University, The Netherlands

[3] Instituto de Medicina Molecular, Lisboa, Portugal

[4] Present address: Department of Biology, Institute of Biochemistry, Swiss Federal Institute of Technology, Zurich, Switzerland

[5] Present address: Laboratorio Nacional de Microscopía Avanzada, Instituto de Biotecnología, Universidad Nacional Autónoma de México, México

[6] Present address: IRB Barcelona, Spain

[7] These authors contributed equally to this work

[8] These authors contributed equally to this work

[9] Corresponding author; email: mdias@igc.gulbenkian.pt

Summary

Centrioles are essential for cilia and centrosome assembly. In centriole-containing cells, centrioles always form juxtaposed to pre-existing ones, a century old observation that motivates a long-standing debate on spatial control of centriole biogenesis. Here, we show that *trans*-autoactivation of Polo-like kinase 4 (PLK4) is a critical early event in centriole biogenesis. A mathematical model suggests this process requires PLK4 accumulation above a threshold concentration. We demonstrate that centrioles promote PLK4 activation through its recruitment and local accumulation. Though centriole removal reduces the proportion of active PLK4, this can be rescued by concentrating PLK4 to the peroxisome lumen. Moreover, we show that at low levels of overexpression, PLK4 only triggers centriole biogenesis at the existing centriole, while higher levels can trigger biogenesis at the centriole as well as anywhere in the cytoplasm (*de novo*). Hence, centrioles promote their assembly locally, and disfavour indiscriminate *de novo* synthesis. Mechanisms involving the local concentration of other centriole components are likely to enforce the formation of new centrioles always juxtaposed to pre-existing ones under physiological conditions.

Introduction

Centrioles are microtubule-based structures essential for cilia and centrosome formation (Bettencourt-Dias and Glover, 2007; Nigg and Stearns, 2011). In each cell cycle one and only one centriole is formed in a highly controlled fashion close to an already existing centriole (canonical biogenesis) (Bettencourt-Dias and Glover, 2007; Nigg and Stearns, 2011). Centrioles can also form in the absence of a pre-existing centriole (*de novo* biogenesis). *De novo* formation is known to occur in insect species with parthenogenic development, i.e. development without fertilization, as oocytes normally lose their centrioles during oogenesis (Cunha-Ferreira et al., 2009). Human cells can also form centrioles *de novo* upon laser ablation of their centrosome (LaTerra et al., 2005). In most circumstances, *de novo* centriole assembly is slower when compared to the canonical pathway, with centrioles forming in highly variable numbers and presumably anywhere in the cell (Cunha-Ferreira et al., 2009). Intriguingly, the presence of a single centriole is sufficient to prevent *de novo* assembly (LaTerra et al., 2005; Marshall et al., 2001). This preference for canonical biogenesis allows the strict control in timing and number, allowing for biogenesis to be regulated by the multitude of signalling proteins, such as p53, that localize to the centrosome (Bettencourt-Dias and Glover, 2007; Nigg and Stearns, 2011). So how do existing centrioles control where new centrioles form? One possibility is that centrioles release an 'inhibitor of centriole biogenesis' (Marshall et al., 2001). Alternatively, pre-existing centrioles might catalyze centriole assembly, perhaps by preferentially recruiting centriole precursors or by locally activating them (Marshall et al., 2001; Rodrigues-Martins et al., 2007). What could be the nature of such inhibitors/catalyzers of new centriole formation? Regulation of Polo Like Kinase 4 (PLK4), a major player in centriole biogenesis, might play a very important role in the spatial regulation of centriole biogenesis. In the absence of PLK4 no centrioles are formed (Bettencourt-Dias et al., 2005; Habedanck et al., 2005). PLK4 in excess triggers multiple centriole formation at the centrosome in cycling cells (canonical

amplification) (Habedanck et al., 2005; Kleylein-Sohn et al., 2007; Rodrigues-Martins et al., 2007) and *de novo* assembly in acentriolar systems, such as *Drosophila* unfertilized eggs (Peel et al., 2007; Rodrigues-Martins et al., 2007). However, *de novo* biogenesis is slower when compared to the canonical centriole biogenesis observed in fertilized *Drosophila* eggs expressing the same levels of PLK4 (Rodrigues-Martins et al., 2007). This supports a model where centrioles catalyze their own assembly and where PLK4 levels, and consequently its activity, are a limiting factor in both canonical and *de novo* centriole formation. As other protein kinases, PLK4 function is likely to be strongly determined by protein concentration and regulation of its kinase activity (Zitouni et al., 2014). It is known that PLK4 levels are controlled by a negative feedback loop mediated by PLK4 *trans*-autophosphorylation on a specific degron sequence downstream of its catalytic domain that is recognized by the SCF-Slimb/βTrCP ubiquitin ligase complex (Cunha-Ferreira et al., 2013; Holland et al., 2010; Klebba et al., 2013). However, little is known about the regulation of its kinase activity. Here, we set out to investigate how PLK4 activity is regulated and whether centrioles might catalyze this process.

Results

Phosphorylation of *Drosophila* PLK4 Thr172 is required for its catalytic activity

Activation of PLK1, the founding member of the Polo family, involves phosphorylation of one critical residue within its T-Loop in the catalytic domain (Archambault and Carmena, 2012; Zitouni et al., 2014), which is highly conserved in PLK4 (Fig. 1A). While different mechanisms may be involved in PLK4 activation, we first asked if this residue in PLK4 had a role in its activation. We observed phosphorylation of the equivalent residue in PLK4 (Threonine 172) using mass spectrometry (not shown). To confirm the role of Thr172 phosphorylation for PLK4 activity, we used two readouts: the ability of PLK4 to *trans*-autophosphorylate in another residue, which is located in its degron (Ser293 (Cunha-Ferreira et al., 2013), Figures 1B), and its

ability to phosphorylate an exogenous substrate (Myelin Basic Protein – MBP, Figure S1A). The catalytic activity of PLK4(T172A), a mutant where Thr172 was mutated to alanine to mimic its non-phosphorylated state, was significantly reduced as compared to PLK4 wild type (WT; Figures 1B and S1A). Kinase dead PLK4 (KD; bears three mutations in the kinase catalytic site: K43M, K22M and D156A (Rodrigues-Martins et al., 2008)) showed no activity as expected. It is important to note that the T172A mutation preventing activation of PLK4 also affected its steady-state stability, as the mutant is much more stable, similarly to a kinase dead PLK4 (Figure S1B). This is consistent with previous studies demonstrating that a catalytically inactive PLK4 is more stable as it cannot autophosphorylate in a degron that targets itself for degradation (Cunha-Ferreira et al., 2013; Holland et al., 2010; Klebba et al., 2013). Moreover, impairment of PLK4´s ability to be phosphorylated at residue Thr172, from hereinafter called 'PLK4 activation', also had strong consequences in its centriole biogenesis function (Figures 1C-D). Similar to the kinase dead, expression of PLK4(T172A) could not rescue the accumulation of cells with an abnormally low number of centrioles (less than 2) that arose from depletion of endogenous PLK4 (Figures 1C-D; category '0-1'). Together, these data suggest that though Thr172 non-phosphorylated PLK4 has residual catalytic activity (Figure 1B), this is not sufficient to drive centriole biogenesis (Figure 1C-D).

PLK4 regulates its own kinase activity by autophosphorylating Thr172

The identity of the kinase that activates PLK4 in an unperturbed cell is hitherto unknown. The activating phosphorylation of the T-loop of a kinase can either be mediated by another kinase (e.g. PLK1 (Zitouni et al., 2014)) or it can be autocatalytic (e.g. Aurora A (Adams, 2003)). Stress-activated protein kinases (SAPKKK (Nakamura et al., 2013)) can phosphorylate human PLK4 Thr170, the equivalent residue to *Drosophila* Thr172 (Figure 1A), upon cellular stress. However, multiple RNAi screens in unperturbed cells failed to identify a kinase whose activity is

required for PLK4´s function (Balestra et al., 2013; Bettencourt-Dias et al., 2005; Brownlee et al., 2011; Dobbelaere et al., 2008; Goshima et al., 2007). Since PLK4 kinase domain can autophosphorylate *in vitro* (Dodson et al., 2013), we therefore proceeded to test whether PLK4 autoactivates in a normal cell cycle.

We generated and tested a phospho-specific antibody (p-PLK4 Thr172) *in vitro* and cycling cell extracts (see loss of signal upon phosphatase treatment and T172A mutation in Figures 2A-B, and S2A). Full length bacterially expressed GST-PLK4(WT) showed Thr172 phosphorylation and reduced gel mobility, suggestive of autophosphorylation, which was not observed upon phosphatase co-expression (λ-ppase) (Shrestha et al., 2012) or expression of kinase dead PLK4 (KD; Figure 2A). These results show that PLK4 kinase catalytic activity is required and sufficient for its autophosphorylation at Thr172 *in vitro*. We observed the same result by adding ATP to dephosphorylated His-MBP-PLK4(WT) (Fig. S2B). Autophosphorylation of Thr172 was observed very early upon ATP addition and increased with time (Fig. S2B), showing that Thr172 dephosphorylated PLK4 has 'residual catalytic activity' thus being able to autophosphorylate. To test whether PLK4 Thr172 autophosphorylation activates PLK4, we compared the catalytic activity of PLK4 species with different levels of phosphorylation in this residue (Figure S2C). Our results show that PLK4 with higher levels of phosphorylation in Thr172 was more efficient in substrate phosphorylation (Figure S2C), suggesting that Thr172 phosphorylation correlates with activity. Although our data does not exclude that full PLK4 activation may be more complex, with other autophosphorylated residues (Klebba et al., 2015a) potentially also playing a role in PLK4 autoactivation, it strongly suggests that Thr172 is an important residue in this function.

Finally, we asked whether PLK4 also autoactivated in cells in an unperturbed cell cycle. We found that Thr172 was not phosphorylated when only the kinase dead (KD) mutant was expressed in the absence of endogenous PLK4 (Figure 2B). Furthermore, we observed the same results even upon expression of very high levels

of PLK4 (PLK4 non-degradable, i.e. that cannot be targeted for degradation, ND, and PLK4 non-degradable kinase dead, KDND (Cunha-Ferreira et al., 2009); Figure 2B). These results show that PLK4 can autoactivate in cells in an unperturbed cell cycle.

Autophosphorylation is common to many kinases, but it can be achieved through multiple molecular mechanisms, which result in different kinetic properties. Mps1, a kinase involved in mitotic checkpoint signalling, autophosphorylates and activates in *trans* (Jelluma et al., 2008; Kang et al., 2007; Mattison et al., 2007). Other kinases, such as p38, autophosphorylate in *cis* (DeNicola et al., 2013). To further understand the kinetics of PLK4 autophosphorylation (*cis vs. trans*), we investigated the level of phosphorylation at Thr172 by adding ATP to different concentrations of dephosphorylated His-MBP-PLK4(WT) (Figure 2C). Autophosphorylation of Thr172 increased nonlinearly with increase in PLK4 concentration (Figure 2C) showing that Thr172-dephosphorylated PLK4 is able to autoactivate in *trans*. To confirm whether PLK4 can autophosphorylate in *trans* in cells at the Thr172 residue we simultaneously expressed GFP-PLK4(WT) and Myc-PLK4(KD) in the absence of endogenous PLK4 (Figures 2D-E). While individually expressed PLK4(WT) is found autophosphorylated at Thr172 (left lane), PLK4(KD) is not (middle lane). However, co-expression of both the active (WT) and inactive kinases (KD) led to phosphorylation of PLK4(KD) at the Thr172 residue (right lane) by the co-expressed active PLK4(WT), demonstrating autophosphorylation in *trans* (Figures 2D-E).

PLK4 activation is dependent on its localized accumulation

To investigate the implications of a PLK4 *trans*-autoactivation mechanism in the spatial regulation of centriole biogenesis, we generated a simple mathematical model of PLK4 activity. This model takes into account the synthesis of a ‘basal form’ of PLK4 (non-Thr172 phosphorylated PLK4 with residual catalytic activity), which is activated through phosphorylation of Thr172 in the T-loop, and subsequently

targeted for degradation by autophosphorylation in the degron (B, A* and A**, respectively, in Figure 3A). We posit two alternative scenarios for PLK4 activation by *cis*- or *trans*-autophosphorylation (Figure 3A-B). In contrast to a scenario in which PLK4 autophosphorylates in *cis* (or is phosphorylated by other unknown kinase), the positive feedback resulting from PLK4 *trans*-autophosphorylation gives rise to a threshold of total PLK4 concentration (Figure 3B) below which there is little PLK4 activation, reflecting the unlikely encounters between two PLK4 molecules.

An important output of incorporating PLK4 *trans*-autoactivation in our model is that PLK4 is only activated when sufficiently concentrated (Figure 2C). Since PLK4 localizes to the centrosome it is possible that the organelle acts as a 'PLK4 concentrator', accumulating the kinase until it reaches supra-threshold concentrations. To assess this possibility, we elaborated a two-compartment model that features an exchange of all PLK4 forms between the cytoplasm and the centrosome (Figure 3C). The model assumes that the volume ratio of the two compartments is 2000 (Decker et al., 2011), the exchange of PLK4 is biased towards the centrosome, and PLK4 basal catalytic activity is twenty times lower than that of the activated PLK4 (phosphorylated at Thr172, Figure 1B). Under these assumptions, the model indicates that normal PLK4 production can be tuned so that it elicits robust PLK4 accumulation and activation at the centrosome while being insufficient to trigger PLK4 activation in the cytoplasm (Figure 3D), thus offering a mechanism to prevent centriole formation in the cytoplasm. If this holds true, the model suggests several outcomes (Figure 3D): i) the absence of PLK4 recruitment to the centrosome should lead to little PLK4 *trans*-autoactivation (Figure 3D, no centrosome and no PLK4 overexpression); ii) concentrating PLK4 elsewhere in the cell should be sufficient to activate it; iii) PLK4 overexpression at low levels should lead to a higher proportion of activated PLK4 at the centrosome and thus canonical amplification, or to *de novo* centriole biogenesis in the absence of the centrosome, as reported before (Rodrigues-Martins et al., 2007) as PLK4 is no longer

sequestered by this organelle (Figure 3D, PLK4 overexpression +); iv) PLK4 overexpression at high levels should produce a higher proportion of active PLK4 forms anywhere in the cytoplasm, therefore eliciting *de novo* biogenesis even in the presence of a pre-existing centrosome, thus overriding the principle of *de novo* biogenesis inhibition by the centrosome (Marshall et al., 2001; Rodrigues-Martins et al., 2007) (Figure 3D, PLK4 overexpression ++). We decided to test all predictions, particularly the ones that had not been tested in the literature, i.e. i), ii) and iv).

The centrosome is the physiological 'PLK4 concentrator'

We experimentally tested whether PLK4 *trans*-activation in Thr172 is dependent on local concentration of PLK4 at the centrosome (prediction i). We first analyzed whether non-phosphorylatable PLK4(T172A) can localize to the centrosome. Indeed, similar to PLK4(WT), PLK4(T172A) localized to the centrosome (Figure 4A). We then tested if abrogation of PLK4 recruitment to the centrosome would prevent its *trans*-activation, by depleting Asterless (Asl, CEP152 in vertebrates), a molecule that is needed for PLK4 recruitment to the centrosome (Cunha-Ferreira et al., 2013; Dzhindzhev et al., 2010), while expressing PLK4(WT) (Figures 4B-E). Interestingly, we have shown in the past that PLK4(KD), which is not phosphorylated in Thr172 (Figure 2), can still interact with Asl (Cunha-Ferreira et al., 2013). Indeed, depletion of *Asl* led to impaired recruitment of PLK4(WT) to the centrosomes (Figures 4B-C) and to the reduction in the number of centrosomes (Figure 4D), as reported before (Dzhindzhev et al., 2010). Concomitantly, we saw a reduction in the ratio of PLK4 phosphorylated in Thr172 (Figure 4E). In agreement with our hypothesis, these results strongly suggest that localization of PLK4 at the centrosome is normally required for its activation. Finally, to further test whether centrosomes are required for PLK4 activation in a more definitive manner, we investigated the ratio of activated PLK4(WT) in normal cells *vs.* acentrosomal cells. In *Drosophila* tissue culture cells we can generate acentrosomal cells by depleting an essential component of the

centriole, SAS-6 (Peel et al., 2007; Rodrigues-Martins et al., 2007) for several rounds of cell division (more than 8 rounds). As cells divide normally without being able to duplicate their centrioles, the population of cells with abnormally low number of centrioles (0-1) increases to almost 100% (Rodrigues-Martins et al., 2007) (*SAS-6* RNAi; Figure 5C). We compared the ratio of activated PLK4 (p-PLK4 Thr172) in GFP-PLK4(WT)-expressing cells with and without centrioles (*mCherry* or *SAS-6* RNAi, respectively; Figure 5D, left panel). Whereas we could detect p-PLK4 Thr172 in cells with centrioles (*mCherry* RNAi), we were unable to detect this activated PLK4 form in acentriolar cells (*SAS-6* RNAi). As PLK4 becomes more active at the centrosome, it is possible that it also autophosphorylates more in its degron, targeting itself for degradation (Cunha-Ferreira et al., 2013; Klebba et al., 2013). In agreement with this, we observed that PLK4 was more stable in acentriolar cells (*SAS-6* RNAi; Figure S3A).

Together, these results strongly support "prediction i" that PLK4 *trans*-activation is normally dependent on its recruitment and concentration at the centrosome, suggesting that the centrosome concentrates PLK4. However, our experiments do not formally exclude the possibility that perhaps a molecular component at the centrosome is catalyzing PLK4 *trans*-autophosphorylation. We therefore tested "prediction ii", i.e. whether concentration of overexpressed PLK4 alone outside of the centrosome is sufficient to promote PLK4 *trans*-autophosphorylation in cells by accumulating it on the peroxisome lumen or artificially on beads.

We targeted PLK4 to the peroxisome lumen using the SKL tag, a C-terminal peroxisome-targeting sequence responsible for the import of the majority of peroxisomal proteins into that organelle (Gould et al., 1989) (Figure 5A). Whereas GFP-PLK4(WT) always localized to the centrosomes, GFP-PLK4(SKL) was scattered in foci throughout the cytoplasm. In 58% of cells GFP-PLK4(SKL) co-localized only with the peroxisomal marker mCherry-SKL, while 39% of the cells

showed co-localization with both the peroxisome and the centrosome (Figure 5B). We then removed the centrosomes from cells as discussed previously, with prolonged *SAS-6* RNAi, so that GFP-PLK4(SKL) could no longer localize to centrosomes but only to peroxisomes, hence focusing on the consequences of localizing PLK4 on a different structure than the centrosome (Figure 5C). Remarkably, we observed a very strong signal for p-PLK4 Thr172 (Figure 5D, middle panel, *SAS-6* RNAi), showing that enforced PLK4 concentration is sufficient to lead to its activation in cells. We also detected an increase in reduced gel mobility forms of total PLK4 when at the peroxisome (GFP-PLK4(SKL); Figure 5D, left and middle panels) suggesting that PLK4 might be shielded from phosphatases and/or the SCF-mediated degradation machinery when concentrated inside that organelle, as opposed to the cytoplasm (GFP-PLK4(WT), *SAS-6* RNAi) and the centrosome (GFP-PLK4(WT), *mCherry* RNAi) ((Brownlee et al., 2011); note that the antibody against total PLK4 does not recognize a fraction of hyper-phosphorylated PLK4 that migrates slowly and is recognized by the p-PLK4-Thr172 antibody). Furthermore, the ratio of Thr172 phosphorylated PLK4 to total PLK4 at the centrosome (PLK4(WT)) and at the peroxisome (PLK4(SKL)) was dependent on PLK4 concentration, as expected (Figure 5E). Though PLK4 was highly active at the peroxisome lumen, we did not observe centriole formation there, likely due to the lack of substrates required for centriole biogenesis within that organelle. In fact, Ana2/STIL, a substrate, and recently shown activator of PLK4 (Moyer et al., 2015), was not observed at the peroxisome (Figure S3B).

Finally, we corroborated these findings by artificially concentrating GFP-PLK4(WT) in beads that bind to more than one GFP molecule. After GFP-PLK4(WT) immunoprecipitation from cellular extracts, with consequent concentration on the beads, we observed an increase in reduced gel mobility forms and Thr172 phosphorylation independently of the presence of centrosomes (Figure 5D, right panel, *mCherry* (with centrosomes) or *SAS-6* (no centrosomes)). We conclude that,

similar to the peroxisome targeting in cells, PLK4-enforced immobilization on beads during immunoprecipitation enables *trans*-autoactivation of PLK4. Together, the experiments above described show that the centrosome is a potent promoter of PLK4 activation and that this likely works in part through recruitment and concentration of PLK4, as replacing the centrosome by the peroxisome or beads rescues PLK4´s *trans*-autoactivation in Thr172.

High levels of PLK4 can overcome the '*de novo* biogenesis inhibition'

Finally, we tested "predictions iii and iv", i.e. that in the presence of centrioles, low levels of PLK4 should promote only canonical amplification, while high levels of PLK4 should overcome the '*de novo* biogenesis inhibition', leading to the very unusual co-occurrence of both canonical and *de novo* amplification. In this case, PLK4 levels would be sufficient to lead to its activation, and consequent centriole biogenesis, anywhere in the cytoplasm.

We chose *Drosophila* spermatogenesis as an experimental system to test our predictions as it provides several advantages (Figure 6A): i) cells within 16-cell cysts are in G_2 and have two centrosomes, each with two very long (1.25 μm) easily detectable centrioles (in inset in Figure 6A) and ii) using Bam promoter (BamGal4) (Chen and McKearin, 2003) we can ectopically overexpress GFP-PLK4 at different levels by simply growing the same flies at different temperatures (from 16ºC to 25ºC) as Gal4 expression is very sensitive to temperature. Indeed, we found that the flies grown at 16ºC and 25ºC overexpress very low and high amounts of PLK4, respectively (Figure 6B). While control flies (with no PLK4 overexpression) consistently showed two wild-type (WT) centrosomes, each with two centrioles, at all temperatures (Type I, shown only for 25ºC in Figure 6C-F), we observed centriole amplification, starting in the 16-cell cyst, in PLK4 overexpressing-flies grown at all temperatures (Figures 6C-D). The number of centrioles increased with PLK4

overexpression levels (Figures 6C-D) with some cells harbouring as many as 25 centrioles (Figure 6D).

At low levels of PLK4 overexpression (16ºC) we found that 25% of the cells had only two centrosomes, each with several centrioles forming a rosette (Type III, Figures 6C,E). Thus, low PLK4 overexpression promotes canonical amplification in spermatocytes, as previously described in many cell types (Cunha-Ferreira et al., 2009; Kleylein-Sohn et al., 2007). Strikingly, in the remaining 75% of the spermatocytes, we detected two rosettes and additional supernumerary clusters of centrioles, each containing one or more centrioles (we called them centrosomes for simplicity, Type IV, Figures 6C,E-F), suggesting the co-occurrence of canonical and *de novo* amplification in the same cell. In agreement with our model, we observed that the number of *de novo* formed centrosomes increased with PLK4 levels (Figures 6E-F), showing that high levels of PLK4 in the cytoplasm lead to formation of *de novo* centrosomes even in the presence of pre-existing centrioles.

Importantly, we never detected *de novo* formed centrioles in the presence of WT centrosomes (with 2 centrioles) (Type II, Figure 6E) at any of the different levels of PLK4 overexpression, suggesting that canonical biogenesis is favoured to *de novo* assembly. This result strongly supports our model in which the centrosome is a natural 'concentrator' of PLK4, thus promoting its activation.

Discussion

Why centrioles normally form close to existing centrioles is an intriguing question that has fuelled debates about the origin of centrioles as self-replicating entities. Here, we asked how control of the activity and local concentration of a major regulator of centriole biogenesis, PLK4, contributes to the spatial control of centriole formation. We show that phosphorylation of the conserved Thr172 T-loop residue is essential for PLK4 kinase activity and function in centriole biogenesis (Figure 1). Furthermore, PLK4 *trans*-autophosphorylates Thr172, hence autoactivates (Figure 2); and as a

consequence PLK4´s activation critically depends on its concentration (Figures 3 and 5). We also demonstrate that the centrosome acts as a natural PLK4 concentrator (Figures 4 and 5), as this role can be substituted by concentrating overexpressed PLK4 on peroxisomes or beads (Figure 5). Our data shows that in a centrosome-containing cell, given the naturally low expression of PLK4, its full activation can only be attained upon concentration at the centrosome, thus explaining why daughter centrioles are formed close to their mothers, thus resembling a self-replicating process (Figure 6 and summarised in the model in Figure 7). We also show that at sufficiently high levels of PLK4 expression, centrosomes no longer inhibit *de novo* formation (Figures 6 and 7).

Our data also explains other conundrums. It suggests that in the absence of the centrosome PLK4 remains in the cytoplasm where it is more stable, thus leading to a higher cytoplasmic concentration than it normally exists in centrosome-containing cells. This setting increases the likelihood of stochastic encounters between *trans*-autoactivating PLK4 molecules in the cytoplasm and consequently favours the *de novo* centriole formation (LaTerra et al., 2005) (Figures 3 and S3). In centrosome-containing cells, however, recruitment of PLK4 to the centrosome disfavours its accumulation and autoactivation in the cytoplasm (Figures 3, 6 and 7), hence preventing the *de novo* synthesis of centrioles. This provides an explanation for why centrosomes do not normally form *de novo* in centrosome-containing cells a phenomenon that was not explained previously (LaTerra et al., 2005; Uetake et al., 2007). In agreement with this, accumulation of active PLK4 by any other means, such as preventing its degradation, should also lead to the observation of *de novo* formed centrioles (Wang et al., 2011). The regulation of centriole biogenesis by PLK4 autophosphorylation is similar to better studied processes of polarity establishment, such as the selection of bud site in budding yeast (Li and Bowerman, 2010). In this system, in the absence of spatial cues, intrinsic mechanisms, including positive feedback loops, amplify small and stochastic asymmetries thus breaking symmetry to

establish polarity and to form a bud. If spatial cues such as bud scars are present, they orient polarity by biasing the site of amplification of asymmetry. Here, the centriole is the entity that biases the site of amplification. Similar local positive feedback circuits may operate in the spatial inheritance of other cellular structures.

We had previously described a negative feedback loop involving PLK4 *trans*-autophosphorylation in a degron that targets PLK4 for degradation through an ubiquitin ligase complex Slimb/β-TRCP (Cunha-Ferreira et al., 2009, 2013). Here, we describe a positive feedback loop where PLK4 activation is positively regulated by its own concentration. Our and others work suggest that PLK4 is translated and recruited to the centrosome where it accumulates (Cizmecioglu et al., 2010; Dzhindzhev et al., 2010; Fode et al., 1996; Hatch et al., 2010; Sillibourne et al., 2010; Sonnen et al., 2012) until it reaches a threshold that quickly leads to full activation of the kinase, which is essential to trigger centriole biogenesis. The active PLK4 will then target itself for degradation (Cunha-Ferreira et al., 2013; Holland et al., 2010; Klebba et al., 2013). It is likely that both activation and degradation of PLK4 at the centrosome and in the cytoplasm might be further regulated by many variables such as: i) phosphorylation of other residues in PLK4 (Klebba et al., 2015a); ii) state of oligomerization of PLK4 (Klebba et al., 2015a, 2015b), iii) interactions with scaffold proteins such as Asl/CEP152 (Klebba et al., 2015b), iv) interactions with its substrates and recently shown activators, such as Ana2/STIL (Moyer et al., 2015; Ohta et al., 2014), with phosphatases (Brownlee et al., 2011), and other proteins (Xu et al., 2014). In the future, it will be critical to study the regulation of the "activating" and degron-phosphorylation events in PLK4, and how they generate a lag time during which PLK4 can be active to phosphorylate its substrates in the right place and at the right time. In addition, it will be important to understand when during the cell cycle PLK4 reaches its critical threshold concentration to trigger centriole assembly and how this is regulated.

Catalysis of centriole biogenesis at existing centrioles may present

advantages to the eukaryotic cell, namely the control of centriole number and localization. In fact, *de novo* centrioles, form in random numbers and locations in cells without pre-existing centrioles (Bettencourt-Dias and Glover, 2007; LaTerra et al., 2005; Rodrigues-Martins et al., 2007; Shang et al., 2002). To our knowledge, centrioles are formed close to existing centrioles in all known species that have centrioles. This is true for species that have centrioles within the context of centrosomes, such as most animals, and also in species that have many centrioles forming cilia (called basal bodies) at the cortex, such as ciliates (Carvalho-Santos et al., 2011). Daughter centrioles form and remain very close to their mothers until mitotic exit, when they come apart and become competent to nucleate daughters. This mechanism ensures centriole duplication only occurs once per cell cycle (Nigg and Stearns, 2011). Therefore, spatial regulation of biogenesis enforces control of centriole number. Spatial control is also important for geometrical organization of the cell and movement, as it defines the localization of microtubule organizing centres, such as the centrosome and cilia/flagella. For example, in the multiciliate *Tetrahymena*, new basal bodies are formed close to their mothers, so that new cilia form within cortical rows with the right orientation in the right place. When centrioles form *de novo* in ciliates, they are not equally distributed across the cortex and the organism can show transient defective motility (Shang et al., 2002).

Is PLK4 the only centriole component whose biochemical properties provide spatial constraints to centriole biogenesis? While the last common ancestor of eukaryotes was likely to have centrioles/basal bodies and molecules that are necessary for its biogenesis, such as SAS-6, PLK4 only exists in Opistokhonts (animals and fungi) (Carvalho-Santos et al., 2010, 2011). It is possible that other kinases, such as the ancestral member of the Polo kinase family, played the same role and was regulated in a similar concentration-dependent manner. However, it is also possible that other components of the centrosome are regulated in a similar fashion; indeed, it was recently shown that human SAS-6 is present in the cytoplasm

primarily as a homodimer and that its oligomerization into a centriole precursor structure occurs at centrioles, where SAS-6 is known to concentrate (Keller et al., 2014). So the local regulation of several centriole components may contribute to the spatial accuracy of centriole biogenesis.

PLK4 is upregulated and associated with bad prognosis in breast cancer and its deregulation causes microcephaly and cancer (Marthiens et al., 2013; Mason et al., 2014). Significantly, inhibitors of this kinase have been recently reported and are now in clinical trials for breast cancer treatment (Mason et al., 2014; Wong et al., 2015). Understanding how PLK4 activity is regulated is thus critical to understand the effects of drugs that target this enzyme, the potential mechanisms of resistance to be counteracted and to rationally define which tumours are drug-sensitive. Markers of PLK4 activity, such as phosphorylation of the activation T-loop residue described in this work, might also be used to aid in patients' stratification for clinical decisions, including whether to enrol in surveillance programs and choice of therapy.

Experimental Procedures

Plasmid constructs

All the vectors used in this study were constructed using the Gateway system (Invitrogen, USA) according to the manufacturer instructions. The pAWM destination vector (with Myc tag and Actin 5C promoter) was acquired at DRGC (Indiana, USA). The pACYC-RIL-λppase for expression in *E. coli* was a kind gift from Dr. Jonathan M. Elkins (Oxford University, UK) (Shrestha et al., 2012). The GFP N-terminal plasmid was a kind gift of João Rocha (University of Cambridge, UK). The PLK4 entry vector has been described elsewhere (Bettencourt-Dias et al., 2005). The GFP C-terminal PLK4(WT) plasmid was a gift from Dr. Gregory C. Rogers (University of Arizona, USA). The mCherry-SKL vector (with Actin 5C promoter) was kindly provided by Vladimir Gelfand (Northwestern University School of Medicine, USA). His-MBP (PET41A) derived from PET22b(+) was a kind gift from Arie Geerlof (EMBL,

Germany). The dicistronic vector pGEX-2RBS (created by Anna De Antoni) was a kind gift from Andrea Musacchio (Milan, Italy) (Ciferri et al., 2005). The pGEX-2RBS-GST-PLK4(WT) and PLK4(KD) have been described elsewhere (Cunha-Ferreira et al., 2013). The PLK4 Kinase Dead (KD) mutant includes three mutations in the PLK4 catalytic domain of PLK4: K43M in the nucleotide binding motif, K22M in the phosphate anchor, and D156A in the activation loop. This mutant has been described elsewhere (Rodrigues-Martins et al., 2008). Non-degradable PLK4(ND) mutant includes two mutations within the DSGIIT degron, S293A and T297A. This mutant has been described in (Cunha-Ferreira et al., 2009). The PLK4(KDND) mutant includes three mutations within the activation segment: K43M, K22M, D156A and two additional mutations within the DSGIIT degron: S293A and T297A. This mutant has been has been described elsewhere (Cunha-Ferreira et al., 2013). To create the PLK4(T172A) and PLK4(SKL) mutants we used the Quick Change XL Site-Directed mutagenesis kit (Stratagene, Santa Clara, USA), according to the manual instructions. The PLK4 entry vector was used to mutate Thr172 to alanine. PLK4(SKL) was constructed by performing site-directed mutagenesis on the PLK4 entry vector to add the tripeptide sequence S (Serine) – K (Lysine) – L (Leucine) at the C-terminus region of PLK4, as previously described (Gould et al., 1989). The primers used for site-directed mutagenesis are listed below. All the constructs were sequenced and confirmed prior to recombination into destination vectors.

List of primers used for PLK4 site-directed mutagenesis		
Name	**Forward (5'-3')**	**Reverse (5'-3')**
PLK4(T172A)	CCTGATGAGCGCCATATGGCCATG TGTGGAACTCCGAAC	GTTCGGAGTTCCACACATGGCCATATG GCGCTCATCAGG

PLK4(SKL)	AATCGCATGCTTCTTAGCAAGCTGT AAGACCCAGCTTTCTTGTAC	GTACAAGAAAGCTGGGTCTTACAGCTT GCTAAGAAGCATGCGATT

Protein depletion and transient plasmid transfection

Drosophila cells (DMEL) were cultured in Express5 SFM (Gibco,USA) supplemented with 1x L-Glutamine-Penicilin-Streptomycin according to standard tissue culture techniques. dsRNA synthesis against *mCherry*, *ePLK4*, *SAS-6* and *Asl* was performed as previously described (Bettencourt-Dias et al., 2004). dsRNA for endogenous *PLK4* (*ePLK4*) was synthesized from genomic DNA with an adjustment of the PCR annealing temperature to 45ºC. For transient transfection of dsRNA, we used 2 million cells and 40 µg of dsRNA. In the case of *ePLK4*, we used a combination of 30 µg of *ePLK4 3'* dsRNA, with 30 µg of *ePLK4 5'* dsRNA. For the respective control experiments, we used 60 µg of *mCherry* dsRNA. Transient transfection with *SAS-6* dsRNA was performed every 4 days during a total period of 12 days. The same protocol was adopted for the corresponding *mCherry* dsRNA control experiments. In *Asl* depletion, two rounds of transient transfection with 30 µg of *Asl* dsRNA every 4 days were performed. *mCherry* dsRNA was used as a control. The primers used for the production of dsRNA are listed below. Transient plasmid transfections were performed with Effectene reagent (Qiagen, USA) according to the manual recommendations. Briefly, 3 million DMEL cells were plated per well (6-well plate) in 1 ml antibiotic-free medium; 400 ng of plasmid DNA were mixed with 3,5 µl Enhancer reagent and incubated for 5 min at RT; 10 µl Effectene transfection reagent were added to the previous solution, mixed and incubated at RT for 10 min; 2 ml antibiotic-free medium were added to the final mix and the solution was added to the cells in a drop wise manner. Transfections proceeded for 4 days at 25ºC. In experiments where the cells had previously been treated with dsRNA, plasmid

transfection was performed on the second day of the depletion. In transient transfections with pMT-derived constructs, induction with $CuSO_4$ was initiated 15 hours before harvesting.

List of primers used for dsRNA synthesis			
Name	**CG number**	**Forward (5'-3')**	**Reverse (5'-3')**
mCherry	-	TAATACGACTCACTATAGGGATG GTGAGCAAGGG	TAATACGACTCACTATAGGGGTT GACGTTGTAGG
Sas-6	15524	TAATACGACTCACTATAGGGAGA TGTAGTGCGCATGCTGAAGGAC	TAATACGACTCACTATAGGGAGA GCTGCGCTGCTCGTTTATTTTG
ePLK4 5'	7186	TAATACGACTCACTATAGGGAGA ATTAATCCCAGGGCTGCATTA	TAATACGACTCACTATAGGGAGA AGCTAGCCTTTTTTCTGTAGAC
ePLK4 3'	7186	TAATACGACTCACTATAGGGAGA TAATTGAATCAAAACTTAATTC	TAATACGACTCACTATAGGGAGA AACCTCACACTTATACAAAAAG
Asl	2919	TAATACGACTCACTATAGGGAGA TTATGGTGAATGCCTTCGAC	TAATACGACTCACTATAGGGAGA CTAGCTCAGCCTGCATGATG

Preparation of whole cell protein extracts

Whole cell lysates were prepared by resupending cell pellets in lysis buffer containing 75 mM HEPES pH 6.8, 150 mM NaCl, 2mM $MgCl_2$, 0.1% NP-40, 5 mM DTT, 5% glycerol, 2 mM EGTA and supplemented with phosphatase inhibitors (200 mM NaF, 150 mM β-glycerophosphate, 1 mM Na_3VO_4) (all chemicals from Sigma, USA) and 1x EDTA-free protease inhibitors (Roche). Laemmli buffer was added to the samples to 1x and then boiled at 99ºC for 5 minutes (min) and centrifuged at 14,000 rpm for 1 min before being analyzed on polyacrylamide gels. The lysate soluble and insoluble fractions were separated by centrifugation at 14,000 rpm for 10

min. The pellet was resuspended in 0.8 M urea and 1x Laemmli buffer. The extract was then boiled at 99ºC for 5 min and centrifuged at 14,000 rpm for 1 min before being analyzed on polyacrylamide gels.

Phosphatase treatments

Whole cell lysates were treated for 30 min at 30ºC with 400 U of lambda phosphatase (New England Biolabs, USA) or lambda phosphatase plus phosphatase inhibitors (already included in the lysis buffer), in 1x phosphatase buffer supplemented with 1 mM $MnCl_2$ (New England Biolabs, USA). After treatment, whole cell extracts were prepared as described in the previous section.

Recombinant PLK4 expression

Recombinant pGEX-2RBS-GST-PLK4(WT), pGEX2RBS-GST-PLK4(WT) and pACYC-RIL λppase, and pGEX2-RBS-GST-PLK4(KD) were each transformed into *Escherichia coli* BL21 cells. PLK4 expression was induced with 1 mM IPTG for 6 hr at 25ºC. For detection of phosphorylated PLK4, the soluble fractions were prepared according to the procedures described above.

***In vitro* auto-phosphorylation of PLK4**

Recombinant dephosphorylated His-MBP-PLK4(WT) was expressed and purified by the Protein Expression and Purification Core Facility, EMBL, Heidelberg, Germany. His-MBP-PLK4 was co-expressed with pACYC-RIL-λppase for dephosphorylation (Shrestha et al., 2012). For *in vitro* autophosphorylation assays, 50 to 800 μM PLK4 were incubated for 10 min at 18ºC in 50 mM Tris-HCl pH 7.5 buffer containing 1 mM ATP and 1 mM $MgCl_2$.

Immunoprecipitation

Ten million cells were transiently transfected with pMT-GFP-PLK4(WT) or pMT-GFP-

PLK4(SKL) and dsRNA against *mCherry* or *SAS-6*, and induced with 150 µM $CuSO_4$ for 15 hours. Cells were harvested and centrifuged at 1000 rpm for 5 min. The pellet was washed in PBS supplemented with protease inhibitors (Roche, USA) and snap frozen in liquid nitrogen. The pellet was then resuspended in 1 ml of lysis buffer and cell lysis was achieved with 4 consecutive freeze-thaw cycles (dry ice and 37ºC water bath). After centrifuging the lysates at 14,000 rpm for 30 min, 80 µl of GFP-Trap beads (Chromotek, Germany) were added to each sample. Protein binding to the beads was performed on a rotating wheel at 4ºC for 3 hours followed by four washes in lysis buffer. PLK4 was retrieved from beads by adding 1x Laemmli buffer in lysis buffer and boiling the samples at 99ºC for 5 min.

Western blotting

Standard western blotting procedures involved blocking in TBS-T (0.1% Triton X-100 in TBS) supplemented with 5% milk powder, and 1% milk powder in TBS-T for antibody incubations and washes. For detection with phospho-specific antibodies, blocking was performed in TBS supplemented with 5% BSA and phosphatase inhibitors (50 mM NaF, and 5 mM Na_3VO_4), primary antibody incubations were performed in TBS-T supplemented with 5% BSA and phosphatase inhibitors and secondary antibody incubations were performed in 5% BSA and phosphatase inhibitors supplemented with 0.01% SDS, while washes were performed in TBS-T.

Immunostaining

DMEL cells were plated onto glass coverslips, allowed to adhere for 1h and post-fixed in 4% formaldehyde in PHEM buffer (60 mM PIPES pH 6.8, 25 mM HEPES pH 7.0, 10 mM EGTA, 4 mM $MgCl_2$). Cells were permeabilized and washed in PBSTB (PBS containing 0.1% Triton X-100 and 1% BSA). Immunostainings were performed as previously described (Rodrigues-Martins et al., 2007). Cells were mounted with a mounting medium containing DAPI to stain DNA (Vectashield, Vector Laboratories,

USA). Cell imaging and centriole scoring were performed on a Leica DMRA2 microscope with a Cool SNAP HQ camera (Photometrics), or with a Nikon Eclipse Ti-E (Nikon) microscope with a Evolve EMCCD camera (Photometrics) and controlled by MetaMorph 7.5 software (Molecular Devices). Images were acquired as a Z-series (0.3 µm z-interval) and are presented as maximal intensity projections. All images were prepared with Adobe Photoshop and Illustrator (Adobe Systems, USA) and ImageJ (NIH, USA). Super-Resolution structured illumination images were acquired using the Zeiss LSM780 ELYRA PS1 (SR-SIM) microscope. All data were captured using a 63x oil objective. ZEISS immersion oil 1.513 was applied. Images were collected and processed using Zeiss Zen software.

Phospho-specific antibodies

Rabbit p-PLK4 Thr172 polyclonal antibody was synthesized, purified and purchased from PhosphoSolutions (Colorado, USA). Short phospho-peptide spanning the Thr172 residue was used for the production of the antibody. Rabbit p-PLK4 Ser293 has been described elsewhere (Cunha-Ferreira et al., 2013). Dot blots were performed against the two antibodies with S293A and T172A mutant phospho-peptides validating these as phospho-antibodies (data not shown). For western blot of whole cell extracts, p-PLK4 Thr172 was used at 1:300 dilutions. To detect bacterially expressed PLK4, p-PLK4 Thr172 and p-PLK4 Ser293 antibodies was used at 1:10000 dilution. All antibodies were supplemented with the corresponding non-phosphorylated peptide at 1000 ng/ml in TBST supplemented with 5% BSA and phosphatase inhibitors for western blot as previously described.

Antibodies

The antibodies used for western blotting were the following: mouse GFP (1:100 dilution, Roche, USA), mouse cMyc (1:500 dilution, clone 9E10, Santa Cruz Biotechnology, USA), mouse GST (1:10000, clone 26H1, Cell Signalling USA),

mouse Histidine (1:2500, Novagen, USA), rabbit actin (1:2000, Sigma, USA), rabbit PLK4 antibody (1:100 dilution (Cunha-Ferreira et al., 2009)), and rabbit Asterless (1:1000, was a kind gift from Dr. David Glover, University of Cambridge, UK). HRP secondary antibodies (Jackson Immunoresearch Laboratories, USA) and IRDye secondary antibodies (Odyssey, LI-COR Biosciences) were used at 1:10000 dilution. The primary antibodies used in immunostaining were the following: chicken anti-*Drosophila*-PLP (1:1000 dilution (Rodrigues-Martins et al., 2007)), mouse cMyc (1:1500 dilution, clone 9E10, Santa Cruz Biotechnology, USA) and rabbit Asterless (1:1000). Secondary antibodies with minimal cross reactivity against other species were used as follows: Rhodamine Redex, FITC, and Cy5 were used at 1:100 dilutions (Jackson Immunoresearch, USA), and Alexa 350 was used at 1:50 dilution (Molecular Probes, USA).

Centrosome scoring

Number codes were assigned to both control and sample slides in order to score centrioles as a blind assay. A total of 100 cells were scored per sample per slide. Cells were categorized according to the number of centrioles (0 to 1, 2 to 4 or more than 4).

Fly stocks and husbandry

Control (RFP::PACT/UASGFP::PLK4; +/+) and PLK4 overexpressing (RFP::PACT/UASGFP::PLK4; BamGal4/+) flies (Cunha-Ferreira et al., 2013) were grown in normal corn meal media at different temperature ranging from 16ºC to 25ºC.

Testes sample preparation, imaging and analysis

To measure the total amount of PLK4, intact testes from 0-1 day old adult males expressing GFP::PLK4 were dissected in testes buffer (183 mM KCl, 47 mM NaCl, 1 mM EDTA and 10 mM Tris-HCl pH 6.8) and fixed in 4% formaldehyde for 20 min.

Intact testes were then washed and mounted using Vectashield (Vector Laboratories, USA) mounting media for imaging. Samples were imaged for GFP::PLK4 on a Leica SPX5 confocal microscope and total GFP fluorescence in the whole testes was measured using Imaris 7.7. To study the centriole amplification, testes from 0-1 day old adults were dissected in testes buffer, transferred to poly-L-lysine glass slides (Sigma, USA), squashed and frozen in liquid nitrogen as previously described (Cenci et al., 1994). Samples were fixed for 8 min in dry ice-cold methanol followed by 10 min in acetone. DNA was stained with DAPI. Testes were mounted using Vectashield (Vector Laboratories, USA) mounting media for imaging. Samples were imaged as a Z-series (0.3 µm z-interval and 0.04 µm XY-pixel size) on a Leica SPX5 confocal microscope. Images are presented as 3D projections using Imaris 7.8.

Acknowledgements

We thank J. Elkins, J. Rocha, G. Rogers, V. Gelfand, A. Geerlof, A. Musacchio and D. Glover for sharing reagents. We thank the IGC imaging unit for help with image acquisition, S. Rosa and the IGC fly facility, and T.M. Bandeiras and the EMBL protein expression unit for their help. We also thank I. Telley, G. Kops, J. Pines, M. Godinho, L. Jansen, C. Nabais, G. Marteil, D. Odde, W. Marshall, R. Oliveira, A. Holland and MBD Lab for discussions and/or for critically reading the manuscript. SCJ and CAML are supported by the FCT (Fundação Portuguesa para a Ciência e Tecnologia) Fellowship SFRH/BPD/87479/2012 and the FCT Project PTDC/BBB-BEP/1724/2012, respectively. The laboratory and MBD are supported by an EMBO installation grant, an ERC starting grant, and grants from the FCT: PFE-GI-UE-ERC-2010-StG-261344, HMSP-CT/SAU-ICT/0075/2009; PTDC/SAU-OBD/105616/2008, FCT-EXPL/BIM-ONC/0830/2013, PTDC/BBB-BEP/1724/2012.

References

Adams, J.A. (2003). Activation Loop Phosphorylation and Catalysis in Protein Kinases: Is There Functional Evidence for the Autoinhibitor Model? Biochemistry *42*, 601–607.

Archambault, V., and Carmena, M. (2012). Polo-like kinase-activating kinases: Aurora A, Aurora B and what else? Cell Cycle *11*, 1490–1495.

Balestra, F., Strnad, P., Fluckiger, I., and Gonczy, P. (2013). Discovering Regulators of Centriole Biogenesis through siRNA-Based Functional Genomics in Human Cells. Dev. Cell *25*, 555–571.

Bettencourt-Dias, M., and Glover, D.M. (2007). Centrosome biogenesis and function: centrosomics brings new understanding. Nat. Rev. Mol. Cell Biol. Cell Biol. *8*, 451–463.

Bettencourt-Dias, M., Giet, R., Sinka, R., Mazumdar, A., Lock, W.G., Balloux, F., Zafiropoulos, P.J., Yamaguchi, S., Winter, S., Carthew, R.W., et al. (2004). Genome-wide survey of protein kinases required for cell cycle progression. Nature *432*, 980–987.

Bettencourt-Dias, M., Rodrigues-Martins, A., Carpenter, L., Riparbelli, M., Lehmann, L., Gatt, M.K., Carmo, N., Balloux, F., Callaini, G., and Glover, D.M. (2005). SAK/PLK4 is required for centriole duplication and flagella development. Curr. Biol. *15*, 2199–2207.

Brownlee, C.W., Klebba, J.E., Buster, D.W., and Rogers, G.C. (2011). The Protein Phosphatase 2A regulatory subunit Twins stabilizes Plk4 to induce centriole amplification. J. Cell Biol. *195*, 231–243.

Carvalho-Santos, Z., Machado, P., Branco, P., Tavares-Cadete, F., Rodrigues-Martins, A., Pereira-Leal, J.B., and Bettencourt-Dias, M. (2010). Stepwise evolution of the centriole-assembly pathway. J. Cell Sci. *123*, 1414–1426.

Carvalho-Santos, Z., Azimzadeh, J., Pereira-Leal, J.B., and Bettencourt-Dias, M. (2011). Evolution: Tracing the origins of centrioles, cilia, and flagella. J. Cell Biol. *194*, 165–175.

Cenci, G., Bonaccorsi, S., Pisano, C., Verni, F., and Gatti, M. (1994). Chromatin and microtubule organization during premeiotic, meiotic and early postmeiotic stages of Drosophila melanogaster spermatogenesis*. J. Cell Sci. *107*, 3521–3534.

Chen, D., and McKearin, D.M. (2003). A discrete transcriptional silencer in the bam gene determines asymmetric division of the Drosophila germline stem cell. Development *130*, 1159–1170.

Ciferri, C., De Luca, J., Monzani, S., Ferrari, K.J., Ristic, D., Wyman, C., Stark, H., Kilmartin, J., Salmon, E.D., and Musacchio, A. (2005). Architecture of the human ndc80-hec1 complex, a critical constituent of the outer kinetochore. J. Biol. Chem. *280*, 29088–29095.

Cizmecioglu, O., Arnold, M., Bahtz, R., Settele, F., Ehret, L., Haselmann-Weiss, U., Antony, C., and Hoffmann, I. (2010). Cep152 acts as a scaffold for recruitment of Plk4 and CPAP to the centrosome. J. Cell Biol. *191*, 731–739.

Cunha-Ferreira, I., Bento, I., and Bettencourt-Dias, M. (2009). From zero to many: control of centriole number in development and disease. Traffic *10*, 482–498.

Cunha-Ferreira, I., Bento, I., Pimenta-Marques, A., Jana, S.C., Lince-faria, M., Duarte, P., Borrego-Pinto, J., Gilberto, S., Amado, T., Brito, D., et al. (2013). Report Regulation of Autophosphorylation Controls PLK4 Self-Destruction and Centriole Number. Curr. Biol. *23*, 2245–2254.

Decker, M., Jaensch, S., Pozniakovsky, A., Zinke, A., Connell, K.F.O., Zachariae, W., Myers, E., and Hyman, A.A. (2011). Limiting Amounts of Centrosome Material Set Centrosome Size in C. elegans Embryos. Curr. Biol. *21*, 1259–1267.

DeNicola, G.F., Martin, E.D., Chaikuad, A., Bassi, R., Clark, J., Martino, L., Verma, S., Sicard, P., Tata, R., Atkinson, R.A., et al. (2013). Mechanism and consequence of the autoactivation p38 α Mitogen-activated Protein Kinase promoted by TAB1. Nat Struct Mol Biol *20*, 1–24.

Dobbelaere, J., Josué, F., Suijkerbuijk, S., Baum, B., Tapon, N., and Raff, J. (2008). A genome-wide RNAi screen to dissect centriole duplication and centrosome maturation in Drosophila. PLoS Biol. *6*, 1975–1990.

Dodson, C.A., Yeoh, S., Haq, T., and Bayliss, R. (2013). A Kinetic Test Characterizes Kinase Intramolecular and Intermolecular Autophosphorylation Mechanisms. Biochemistry *6*, 1–14.

Dzhindzhev, N.S., Yu, Q.D., Weiskopf, K., Tzolovsky, G., Cunha-Ferreira, I., Riparbelli, M., Rodrigues-Martins, A., Bettencourt-Dias, M., Callaini, G., and Glover, D.M. (2010). Asterless is a scaffold for the onset of centriole assembly. Nature *467*, 714–718.

Fode, C., Binkert, C., and Dennis, J.W. (1996). Constitutive Expression of Murine Sak-a Suppresses Cell Growth and Induces Multinucleation. Mol. Cell. Biol. *16*, 4665–4672.

Goshima, G., Wollman, R., Goodwin, S.S., Zhang, N., Scholey, J.M., Vale, R.D., and Stuurman, N. (2007). Genes Required for Mitotic Spindle Assembly in Drosophila S2 Cells. Science (80-.). *316*, 417–421.

Gould, S.J., Keller, G., Hosken, N., Wilkinson, J., and Subramani, S. (1989). A Conserved Tripeptide Sorts Proteins to Peroxisomes. J. Cell Biol. *108*, 1657–1664.

Habedanck, R., Stierhof, Y.-D., Wilkinson, C.J., and Nigg, E.A. (2005). The Polo kinase Plk4 functions in centriole duplication. Nat. Cell Biol. *7*, 1140–1146.

Hatch, E.M., Kulukian, A., Holland, A.J., Cleveland, D.W., and Stearns, T. (2010). Cep152 interacts with Plk4 and is required for centriole duplication. J. Cell Biol. *191*, 721–729.

Holland, A.J., Lan, W., Niessen, S., Hoover, H., and Cleveland, D.W. (2010). Polo-like kinase 4 kinase activity limits centrosome overduplication by autoregulating its own stability. J. Cell Biol. *188*, 191–198.

Jelluma, N., Brenkman, A.B., McLeod, I., Yates, J.R., Cleveland, D.W., Medema, R.H., and Kops, G.J.P.L. (2008). Chromosomal instability by inefficient Mps1 auto-activation due to a weakened mitotic checkpoint and lagging chromosomes. PLoS One *3*, e2415.

Kang, J., Chen, Y., Zhao, Y., and Yu, H. (2007). Autophosphorylation-dependent activation of human Mps1 is required for the spindle checkpoint. Proc. Natl. Acad. Sci. U. S. A. *104*, 20232–20237.

Keller, D., Orpinell, M., Olivier, N., Wachsmuth, M., Mahen, R., Wyss, R., Hachet, V., Ellenberg, J., Manley, S., and Gönczy, P. (2014). Mechanisms of HsSAS-6 assembly promoting centriole formation in human cells. J. Cell Biol. *204*, 697–712.

Klebba, J.E., Buster, D.W., Nguyen, A.L., Swatkoski, S., Gucek, M., Rusan, N.M., and Rogers, G.C. (2013). Polo-like kinase 4 autodestructs by generating its Slimb-binding phosphodegron. Curr. Biol. *18*.

Klebba, J.E., Buster, D.W., Mclamarrah, T.A., Rusan, N.M., and Rogers, G.C. (2015a). Autoinhibition and relief mechanism for Polo-like. Proc. Natl. Acad. Sci. U. S. A.

Klebba, J.E., Galletta, B.J., Nye, J., Plevock, K.M., Buster, D.W., Hollingsworth, N.A., Slep, K.C., Rusan, N.M., and Rogers, G.C. (2015b). Two Polo-like kinase 4 binding domains in Asterless perform distinct roles in regulating kinase stability. J. Cell Biol. *208*, 401–414.

Kleylein-Sohn, J., Westendorf, J., Le Clech, M., Habedanck, R., Stierhof, Y.-D., and Nigg, E.A. (2007). Plk4-induced centriole biogenesis in human cells. Dev. Cell *13*, 190–202.

LaTerra, S., English, C.N., Hergert, P., McEwen, B.F., Sluder, G., and Khodjakov, A. (2005). The de novo centriole assembly pathway in HeLa cells: cell cycle progression and centriole assembly/maturation. J. Cell Biol. *168*, 713–722.

Li, R., and Bowerman, B. (2010). Symmetry Breaking in Biology. Cold Spring Harb. Perspect. Biol. *2*, 1–6.

Marshall, W.F., Vucica, Y., and Rosenbaum, J.L. (2001). Kinetics and regulation of de novo centriole assembly: Implications for the mechanism of centriole duplication. Curr. Biol. *11*, 308–317.

Marthiens, V., Rujano, M.A., Pennetier, C., Tessier, S., Paul-gilloteaux, P., and Basto, R. (2013). Centrosome amplification causes microcephaly. Nat. Cell Biol. *15*, 731–740.

Mason, J.M., Lin, D.C., Wei, X., Che, Y., Yao, Y., Kiarash, R., Cescon, D.W., Fletcher, G.C., Awrey, D.E., Bray, M.R., et al. (2014). Functional Characterization of CFI-400945, a Polo-like Kinase 4 Inhibitor, as a Potential Anticancer Agent. Cancer Cell *26*, 163–176.

Mattison, C.P., Old, W.M., Steiner, E., Huneycutt, B.J., Resing, K.A., Ahn, N.G., and Winey, M. (2007). Mps1 activation loop autophosphorylation enhances kinase activity. J. Biol. Chem. *282*, 30553–30561.

Moyer, T.C., Clutario, K.M., Lambrus, B.G., Daggubati, V., and Holland, A.J. (2015). Binding of STIL to Plk4 activates kinase activity to promote centriole assembly. J. Cell Biol. *209*, 863–878.

Nakamura, T., Saito, H., and Takekawa, M. (2013). SAPK pathways and p53 cooperatively regulate PLK4 activity and centrosome integrity under stres. Nat. Commun. *4*, 1713–1775.

Nigg, E.A., and Stearns, T. (2011). The centrosome cycle: Centriole biogenesis, duplication and inherint asymmetries. Nat. Cell Biol. *13*, 1154–1160.

Ohta, M., Ashikawa, T., Nozaki, Y., Kozuka-hata, H., Goto, H., Inagaki, M., Oyama, M., and Kitagawa, D. (2014). Direct interaction of Plk4 with STIL ensures formation of a single procentriole per parental centriole. Nat. Commun. *5*, 1–12.

Peel, N., Stevens, N.R., Basto, R., and Raff, J.W. (2007). Overexpressing centriole-replication proteins in vivo induces centriole overduplication and de novo formation. Curr. Biol. *17*, 834–843.

Rodrigues-Martins, A., Riparbelli, M., Glover, D.M., and Bettencourt-Dias, M. (2007). Revisiting the role of the mother centriole in centriole biogenesis. Science (80-.). *316*, 1046–1051.

Rodrigues-Martins, A., Riparbelli, M., Callaini, G., Glover, D.M., and Bettencourt-Dias, M. (2008). From centriole biogenesis to cellular function: Centrioles are essential for cell division at critical developmental stages. Cell Cycle *7*, 11–16.

Shang, Y., Li, B., and Gorovsky, M.A. (2002). Tetrahymena thermophila contains a conventional gamma-tubulin that is differentially required for the maintenance of different microtubule-organizing centers. J. Cell Biol. *158*, 1195–1206.

Shrestha, A., Hamilton, G., O'Neill, E., Knapp, S., and Elkins, J.M. (2012). Analysis of conditions affecting auto-phosphorylation of human kinases during expression in bacteria. Protein Expr. Purif. *81*, 136–143.

Sillibourne, J.E., Tack, F., Vloemans, N., Boeckx, A., Thambirajah, S., Bonnet, P., Ramaekers, F.C.S., Bornens, M., and Grand-perret, T. (2010). Autophosphorylation of Polo-like Kinase 4 and Its Role in Centriole Duplication. Mol. Biol. Cell *21*, 547–561.

Sonnen, K.F., Schermelleh, L., Leonhardt, H., and Nigg, E.A. (2012). 3D-structured illumination microscopy provides novel insight into architecture of human centrosomes. Biol. Open *1*, 965–976.

Uetake, Y., Loncarek, J., Nordberg, J.J., English, C.N., La Terra, S., Khodjakov, A., and Sluder, G. (2007). Cell cycle progression and de novo centriole assembly after centrosomal removal in untransformed human cells. J. Cell Biol. *176*, 173–182.

Wang, W., Soni, R.K., Uryu, K., and Tsou, M.B. (2011). The conversion of centrioles to centrosomes: essential coupling of duplication with segregation. J. Cell Biol. *193*, 727–739.

Wong, Y.L., Anzola, J. V, Davis, R.L., Yoon, M., Motamedi, A., Kroll, A., Seo, C.P., Judy, E., Kim, S.K., Mitchell, J.W., et al. (2015). Reversible centriole depletion with an inhibitor of Polo-like kinase 4. Science (80-.). *4*, 1–9.

Xu, Q., Zhang, Y., Xiong, X., Huang, Y., Salisbury, J.L., Hu, J., and Ling, K. (2014). PIPKIγ targets to the centrosome and restrains centriole duplication. J. Cell Sci. *127*, 1293–1305.

Zitouni, S., Nabais, C., Jana, S.C., Guerrero, A., and Bettencourt-dias, M. (2014). Polo-like kinases: structural variations lead to multiple functions. Nat. Rev. Mol. Cell Biol. Cell Biol. *15*, 433–452.

Figure Legends

Figure 1 *Drosophila* PLK4 Thr172 is a conserved phosphorylation site required for kinase activity. **A)** Schematic representation of Drosophila PLK4 showing the Kinase domain, the Cryptic Polo-Box (PB1 and PB2) and the Polo-Box 3 (PB3). The sequence alignment of part of human (Hs) and *Drosophila* (Dm) PLK1 and PLK4 activation segment is also represented. The threonine residue within the T-loop whose phosphorylation leads to PLK1 activation (Thr210/Thr182 in human and *Drosophila* PLK1, respectively) is highly conserved in PLK4 (Thr170/Thr172 in human and *Drosophila* PLK4, respectively). These residues are highlighted in red. **B)** PLK4 T172A mutant has residual catalytic activity. Expression of pMT-GFP-PLK4(WT) (wild-type), GFP-PLK4(T172A) (Thr172 mutated to alanine) and GFP-PLK4(KD) (kinase dead) after depletion of endogenous *PLK4* (*ePLK4* RNAi) in DMEL cells. Cell extracts were prepared and analyzed by western blot with p-PLK4 Ser293 and GFP antibodies. Note that PLK4(WT) was loaded in excess to have similar amounts of the different constructs and thus facilitate comparison of the proportion of p-PLK4 Ser293 (see also Figure S1B). Autophosphorylation at the Ser293 residue (p-PLK4 Ser293) is used as a read-out of PLK4 activity as shown previously (Cunha-Ferreira et al., 2013). Quantification of the ratio of PLK4 phosphorylated at Ser293 to the total amount of PLK4 (GFP-PLK4) is shown. The ratios were normalized to the WT kinase. Data are the average of 3 experiments ± SEM (* $p<0.05$, ** $p<0.01$, t-test). (See also Figure S1A.) **C-D)** PLK4 T172A mutant expression cannot rescue loss of PLK4. **C)** Representative images of immunostaining of DMEL cells expressing act5-Myc-PLK4(WT), Myc-PLK4(T172A) or Myc-PLK4(KD) (in green) after depletion of endogenous *PLK4* (*ePLK4* RNAi). D-PLP (*Drosophila* Pericentrin-Like Protein, a centriole marker, in red) and DAPI (DNA, in blue). Individual cells are outlined by dashed lines that represent the cell outline as judged by the D-PLP background signal. Transfected cells are indicated with an arrow. Note that T172A forms some agglomerates in the cytoplasm, as described

previously for KD (Klebba et al., 2013). Scale bar, 5 µm. **D)** Quantification of centriole number per cell. Data are the average of 3 experiments ± SEM. PLK4(T172A) and PLK4(KD) phenotype of '0-1' is statistically different from that of PLK4(WT) (*** $p<0.0001$, Pearson's χ^2 test). Note that while PLK4(WT) can rescue PLK4 depletion phenotype, PLK4(T172A) cannot. Similar results in centriole biogenesis were obtained using pMT-GFP-PLK4 constructs (WT, T172A and KD) (not shown).

Figure 2 *Drosophila* PLK4 *trans*-autophosphorylates the T-loop residue Thr172. **A)** PLK4 autophosphorylates Thr172 directly in bacteria. Soluble fractions of GST-PLK4(WT), co-expressed or not with λ−ppase, and GST-PLK4(KD) were probed by western blot with p-PLK4 Thr172 and GST antibodies. Phosphorylation of Thr172 was detected in PLK4(WT), whereas there is no detectable phosphorylation in PLK4(WT) when co-expressed with λ−ppase, or in PLK4(KD). Note that PLK4(WT) is hyperphosphorylated as there are no phosphatases in bacteria. **B)** PLK4 catalytic activity is needed for Thr172 phosphorylation in cells. Expression of pMT-GFP-PLK4(WT), GFP-PLK4(T172A), GFP-PLK4(KD), GFP-PLK4(ND) (non-degradable) and GFP-PLK(KDND) after depletion of endogenous *PLK4* (*ePLK4* RNAi) in DMEL cells. Cell extracts were prepared and analyzed by western blot with p-PLK4 Thr172 and GFP antibodies. PLK4(WT) was loaded in excess to have similar amounts of the different constructs and thus facilitating comparison of the proportion of p-PLK4 Thr172 (see also Figure S1B). Note that only PLK4(WT) and PLK4(ND) are phosphorylated at Thr172. Quantification of the ratio of PLK4 phosphorylated at Thr172 to the total amount of PLK4 (GFP-PLK4) is shown. The ratios were normalized to the WT kinase. Data are the average of 3 experiments ± SEM (n.s. not significant, * $p<0.05$, ** $p<0.01$, t-test). Note that the T172A lane does not show pThr172 signal, attesting to the specificity of the antibody (see also Figure S2A regarding the specificity of the antibody). **C)** PLK4 *trans*-autophosphorylates the

Thr172 residue *in vitro*. Autophosphorylation of increasing concentrations of purified dephosphorylated His-MBP-PLK4 (50 to 800 μM) 10 minutes after addition of ATP. Samples were probed by western blot with antibodies against p-PLK4 Thr172 and His (for total PLK4). Quantifications of the intensity of His-PLK4 phosphorylated at Thr172 and of the intensity of total His-PLK4 are shown. The values were normalized to the highest concentration analysed. Note that PLK4 autophosphorylation (p-PLK4 Thr172) shows a trans, non-linear like behavior, different from the PLK4 total levels curve. (See also Figure S2B-C.) **D-E**) PLK4 *trans*-phosphorylates at Thr172 in cells. **D)** Schematic representation of PLK4 *trans*-phosphorylation experiment. **E)** Combinations (as indicated) of pMT-GFP-PLK4(WT), act5-Myc-PLK4(KD), pMT-GFP(empty) and act5-Myc(empty) constructs were expressed in DMEL cells after depletion of endogenous *PLK4*. Cell extracts were prepared and analyzed by western blot with antibodies against GFP to detect GFP-PLK4(WT) and Myc to detect Myc-PLK4(KD). Note that in the presence of PLK4(WT), PLK4(KD) becomes phosphorylated (lower mobility bands) as detected by the use of p-PLK4 Thr172 antibody (lower panel).

Figure 3 Modelling of PLK4 autophosphorylation and the effect of centrosome-dependent concentration of PLK4 on its activation. A) Reaction diagrams representing the *cis*- and *trans*-autophosphorylation of PLK4 (left and right panels, respectively) from a non-Thr172 phosphorylated 'basal form' with residual catalytic activity (B, in grey) to an activated form phosphorylated in the T-loop residue Thr172 (A*, in green), and to doubly phosphorylated form targeted for degradation (A**, in green). The dark arrows indicate the critical flux regulated by either *cis*- or *trans*-phosphorylation. The dashed arrows indicate the kinases catalyzing the phosphorylation steps. When the catalyst and the substrate are the same, the phosphorylation is in *cis* and described as a first order, linear kinetic. When the catalyst and substrate differ the kinetics is non linear. The top arrow describes the

translated PLK4 that enters the system. Lateral, outgoing arrows describe constitutive (thinner) and both constitutive and degron-induced (thicker) elimination of PLK4. **B)** Stable steady state concentrations of the activated and degradation-targeted PLK4 (measured as $A=A^{*}+A^{**}$) as a function of the rate of PLK4 expression (parameter s) in a *cis*-autophosphorylation (continuous red line) and in a *trans*-autophosphorylation mode (continuous green line). **C)** Reaction diagram representing the *trans*-autophosphorylation of PLK4 in a two-compartment model describing the conversion between the three PLK4 forms and their partitioning between the cytoplasm and the centrosome. **D)** The pie charts represent the proportion of basal (in grey) and activated (in green) forms both in the cytoplasm and centrosome, in the presence ('+ Centrosome', left) and in the absence of centrosome ('- Centrosome', right). Three scenarios are illustrated: normal PLK4 production rate in the wild type (s = 0.1, top panel, -), moderate over expression (s = 1, middle panel, +) and strong overexpression (s = 10, bottom panel, ++). Note that: i) the proportion of activated PLK4 is always higher at the centrosome than cytoplasm; ii) within the same levels of overexpressed PLK4 (+ or ++), removal of the centrosome leads to an increase in the proportion of activated PLK4 in the cytoplasm; iii) only high overexpression of PLK4 (++) leads to a high proportion of activated species in the cytoplasm in the presence of a centrosome; iv) if PLK4 is not overexpressed (-) the proportion of activated species in the cytoplasm is not increased upon centrosome removal. The remaining parameters values were: a = 40, b = 2, α = 40, c = 5, p = 10, d = 1, d_c = 40, ρ = 2000, r_1 = 5 parameters r_2 = 1. For detailed description of the models see supplementary information.

Figure 4 Localization of PLK4 to the centriole is important for its activation. A) PLK4(T172A) can localize to the centrosome. Structured illumination images of DMEL cells expressing pMT-PLK4(WT)-GFP and GFP-PLK4(T172A) after depletion of endogenous *PLK4* (*ePLK4* RNAi). Cells were immunostained with antibodies

against Asterless (Asl, in red) and D-PLP (in blue). Note that both PLK4(WT) and PLK4(T172A) localize to the centrioles. Individual cells are outlined by dashed lines that represent the cell outline as judged by the D-PLP background signal. Enlargements of the centrosomes indicated by the arrowheads are shown. Scale bar, 5 µm. **B-E)** Delocalization of PLK4 from the centrosome, through Asl depletion, leads to its reduced activation. DMEL cells were depleted of *Asl* (*Asl* RNAi) (*mCherry* RNAi was used as a negative control) for 4 days, after depletion of endogenous *PLK4* (*ePLK4* RNAi), and followed by transient transfection with pMT-PLK4(WT)-GFP. **B)** Representative structured illumination images. Asl in red, D-PLP in blue. Insets show magnification of centriole. Individual cells are outlined by dashed lines that represent the cell outline as judged by the D-PLP background signal. Enlargements of the centrosomes indicated by the arrowheads are shown. Scale bar, 5 µm. **C)** Cell extracts were prepared and analyzed by western blot. Depletion of *Asl* was confirmed using actin as a loading control. **D)** Quantification of centriole number per cell. Data are the average of 3 experiments ± SEM. Note that '0-1' phenotype in *Asl* depletion is statistically different from that of the control (*mCherry* RNAi) (*** $p<0.0001$, Pearson's χ^2 test). **E)** Cell extracts were prepared and analysed by western blot. Activity of PLK4 at Thr172 was assessed using antibodies against p-PLK4 Thr172 and GFP. *mCherry* control sample was loaded in excess to facilitate the comparison of the proportion of p-PLK4 Thr172. Quantification of the ratio of PLK4 phosphorylated at Thr172 to the total amount of PLK4 (PLK4-GFP) is shown. The ratios were normalized to the control. Data are the average of 3 experiments ± SEM (* $p<0.05$, t-test).

Figure 5 Concentrating PLK4 is sufficient for its activation. A) Construction of *Drosophila* PLK4 with tripeptide targeting it to the peroxisome (SKL). **B**) PLK4(SKL) is targeted to the peroxisome. Immunostaining of DMEL cells expressing pMT-GFP-PLK4(WT) or GFP-PLK4(SKL) and act5-mCherry-SKL (peroxisomal marker, in red)

with D-PLP (in blue). Percentage of cells with PLK4(SKL) localising to the peroxisome (P), centrosome (C) and both peroxisome and centrosome (P+C) is indicated in each merged image. Individual cells are outlined by dashed lines that represent the cell outline as judged by the D-PLP background signal. Enlargements of the indicated areas (squares) are shown. Scale bar, 10 μm. **C-D)** PLK4 is activated at the peroxisome and on beads. Expression of pMT-GFP-PLK4(WT) or GFP-PLK4(SKL) (peroxisome-targeted PLK4) after depletion of *SAS-6* (*SAS-6* RNAi) (*mCherry* RNAi used as a negative control) in DMEL cells for 12 days. **C)** Quantification of centriole number per cell. Note that '0-1' phenotype in *SAS-6* depletion is statistically different from that of the control (*mCherry* RNAi) (*** $p<0.0001$, Pearson's χ^2 test). **D)** Cell extracts were prepared and analyzed by western blot with p-PLK4 Thr172 and PLK4 antibodies. *mCherry* control samples were loaded in excess to have similar amount of PLK4 and thus facilitating comparison of the proportion of p-PLK4 Thr172 (see also Figure S3). GFP-PLK4(WT) was immunoprecipitated and sequentially detected on western blot with p-PLK4 Thr172 and PLK4 antibodies. Quantification of the ratio of PLK4 phosphorylated at Thr172 to the total amount of PLK4 is shown. The ratios were normalized to *mCherry* GFP-PLK4(WT) control. **E)** PLK4 Thr172 phosphorylation is proportional to PLK4 concentration. Peroxisome-targeted PLK4 is more phosphorylated in Thr172. Increased levels of expression of pMT-GFP-PLK4(SKL) in DMEL cells shows that PLK4(SKL) has increased kinase activity as measured by western blot with the p-PLK4-Thr172 antibody. PLK4 antibody was used for total PLK4 detection. The ratios of p-PLK4-Thr172 to the total amount of PLK4 loaded are shown. The ratios were normalized to the 150 μM $CuSO_4$-induced GFP-PLK4(WT) control. We used all PLK4 bands detected, including all the reduced gel mobility bands, for quantification in D and E.

Figure 6 High levels of PLK4 can overcome the inhibition of *de novo* biogenesis. A) Schematic representation of early stages of *Drosophila* spermatogenesis. The division of a stem cell originates a gonial cell that undergoes four rounds of incomplete mitotic divisions to produce a cyst of 16 primary spermatocytes. Primary spermatocytes undergo a long G_2 phase, during which two pairs of centrioles elongate to form very long centrioles (~1.25 μm). **B)** PLK4 overexpression levels can be controlled *in vivo*. Quantification of total overexpressed GFP-PLK4 levels in whole mounted testes of flies grown at different temperatures ranging from 16ºC to 25ºC. a.u., arbitrary units. **C-F)** Varying levels of PLK4 overexpression lead to different pathways of centriole assembly *in vivo*. **C)** Representative images of primary spermatocytes overexpressing different levels of GFP-PLK4. A representative image of a control spermatocyte grown at 25ºC is shown. Control flies always displayed these features at all temperatures (data not shown). Centrioles and DNA are marked using RFP-PACT (PACT is the centriole-targeting domain of *Drosophila* pericentrin, red) and DAPI (blue), respectively. Insets show enlargements of the centrosomes indicated by the arrowheads. Scale bar, 5 μm. **D)** Quantification of the total number of centrioles per spermatocyte from the flies grown at different temperatures ranging from 16ºC to 25ºC. **E)** The histogram shows the percentage distribution of all different cell types observed, classified according to their number of centrosomes and centrioles. All spermatocytes were classified into four categories: 1) Type I: spermatocytes containing only two centrosomes, each consisting of two centrioles. Note that this category was only observed in control cells. 2) Type II: spermatocytes having more than two centrosomes: two with WT-like configuration (containing two centrioles), others containing only single centrioles. Note that we never observed this type of cells. 3) Type III: spermatocytes showing only two centrosomes, each containing supernumerary centrioles, i.e, 3 to 7 centrioles in a rosette-like configuration. 4) Type IV: spermatocytes containing at least 3 centrosomes: two in a rosette-like configuration and the remaining

centrosome containing 1 to 7 centrioles. While it is formally possible that some centrioles could break from a rosette and reduplicate further, we saw supernumerary centrosomes early in the 16 cells stage supporting the conclusion that most clusters are formed *de novo*. Presently, it is also difficult to assert whether the *de novo* formed centrioles within a centrosome form all at the same time or whether some centriole(s) form *de novo* and others subsequently amplify canonically within a centrosome. **F)** Quantification of the total number of supernumerary centrosomes (i.e. additional to the 2 centrosomes observed in WT cells) observed per spermatocyte at different PLK4 levels. The centriole numbers in these centrosomes vary from 1 to 7. Error bars represent ± SD in all graphs.

Figure 7 Distribution of active PLK4 controls different pathways of centriole assembly in the cell. Schematic representation of the different pathways of centriole formation in cells with **(A)** and without **(B)** pre-existing centrioles, according to varying levels of PLK4. **A)** In a cell with a pre-existing centriole, we described three possibilities of centriole formation in this manuscript: i) in wild type cells, endogenously expressed PLK4 is concentrated and thus activated at the existing centriole, leading to canonical centriole biogenesis; ii) at low levels of PLK4 overexpression (OE), higher amounts of PLK4 concentrate and activate at the existing centriole, therefore promoting canonical centriole amplification (rosette-like), iii) at higher levels of PLK4 overexpression, PLK4's concentration is sufficient to promote its activation at the centrosome as well as in the cytoplasm, leading to both canonical and *de novo* amplification. **B)** In a cell naturally without centrioles, such as the wild type unfertilized *Drosophila* egg, PLK4 is expressed at endogenous levels and no centrioles are formed *de novo* (Rodrigues-Martins et al., 2007); upon PLK4 overexpression, *de novo* amplification occurs (Rodrigues-Martins et al., 2007), presumably because PLK4 levels in the cytoplasm are sufficiently high to activate itself. Note that in human cultured cells *de novo* centrioles biogenesis can occur after

laser ablation of pre-existing centrioles without overexpression of PLK4 (LaTerra et al., 2005). The mechanism underlying this phenomenon is still unknown; perhaps these cells have intrinsically higher endogenous PLK4 levels, or centrosome removal could lead to up-regulation of PLK4.

Figure 1

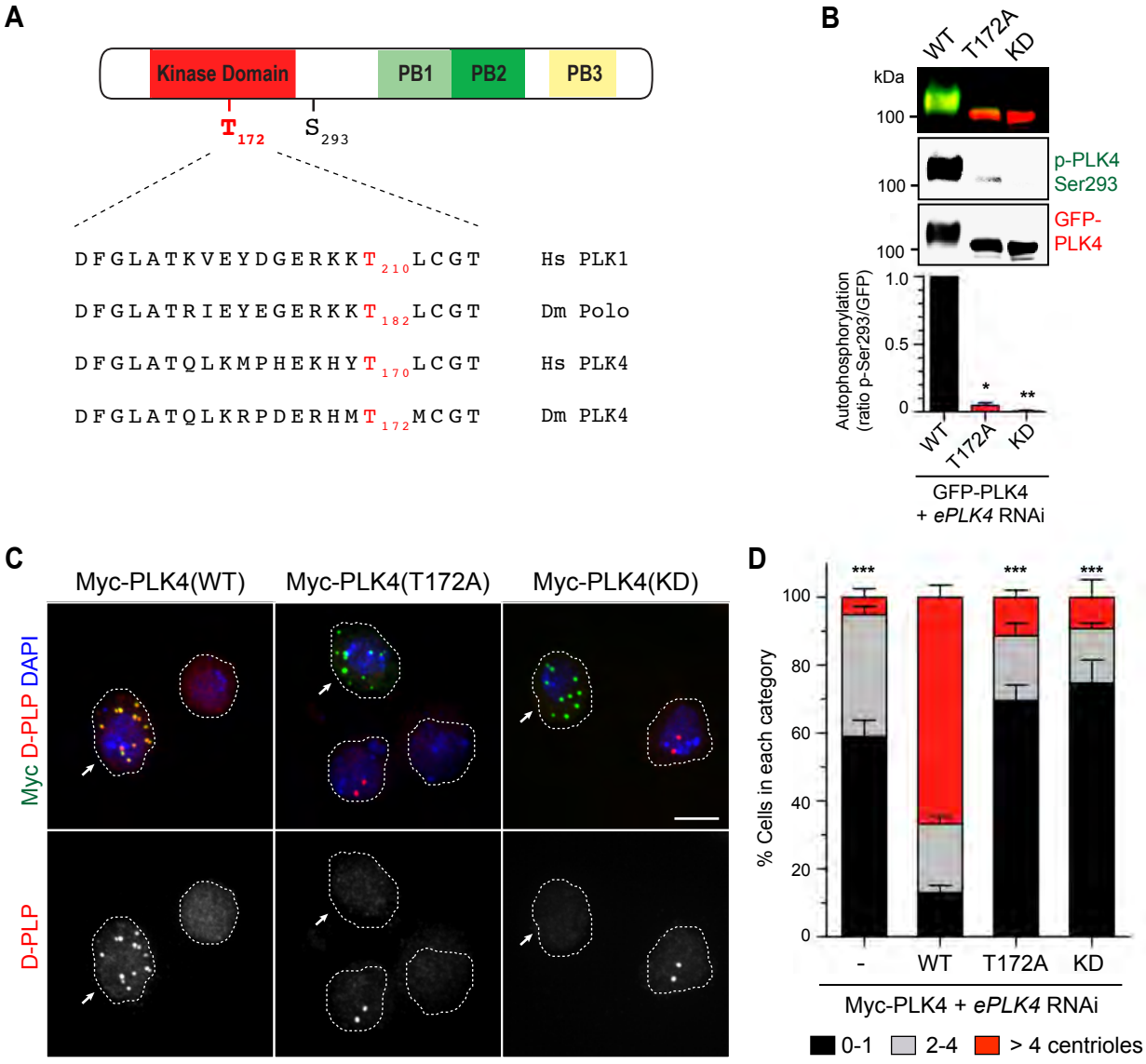
A
Kinase Domain
PB1
PB2
PB3
T172
S293
DFGLATKVEYDGERKKT210LCGT Hs PLK1
DFGLATRIEYEGERKKT182LCGT Dm Polo
DFGLATQLKMPHEKHYT170LCGT Hs PLK4
DFGLATQLKRPDERHMT172MCGT Dm PLK4
B
WT
T172A
KD
kDa
100
p-PLK4 Ser293
GFP-PLK4
Autophosphorylation (ratio p-Ser293/GFP)
1.0
0.5
0
*
**
GFP-PLK4 + ePLK4 RNAi
C
Myc-PLK4(WT)
Myc-PLK4(T172A)
Myc-PLK4(KD)
Myc D-PLP DAPI
D-PLP
D
% Cells in each category
***
Myc-PLK4 + ePLK4 RNAi
0-1
2-4
> 4 centrioles

Figure 2

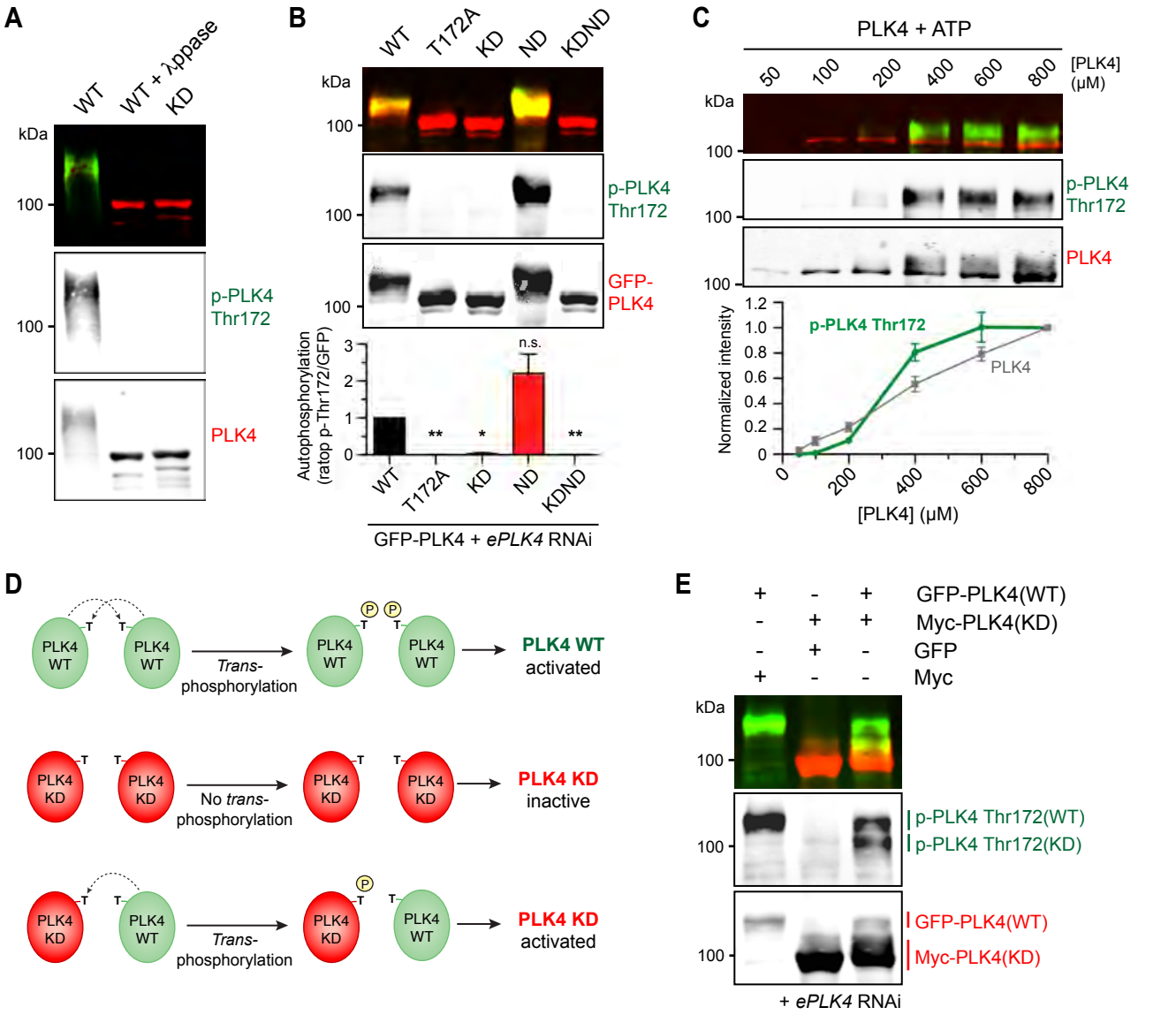
A
WT
WT + λppase
KD
kDa
100
p-PLK4 Thr172
PLK4
B
WT
T172A
KD
ND
KDND
kDa
100
p-PLK4 Thr172
GFP-PLK4
Autophosphorylation (ratop p-Thr172/GFP)
n.s.
**
*
**
GFP-PLK4 + ePLK4 RNAi
C
PLK4 + ATP
50
100
200
400
600
800
[PLK4] (μM)
kDa
p-PLK4 Thr172
PLK4
Normalized intensity
[PLK4] (μM)
D
PLK4 WT
Trans-phosphorylation
PLK4 WT activated
PLK4 KD
No trans-phosphorylation
PLK4 KD inactive
PLK4 KD activated
E
GFP-PLK4(WT)
Myc-PLK4(KD)
GFP
Myc
kDa
p-PLK4 Thr172(WT)
p-PLK4 Thr172(KD)
GFP-PLK4(WT)
Myc-PLK4(KD)
+ ePLK4 RNAi

Figure 3

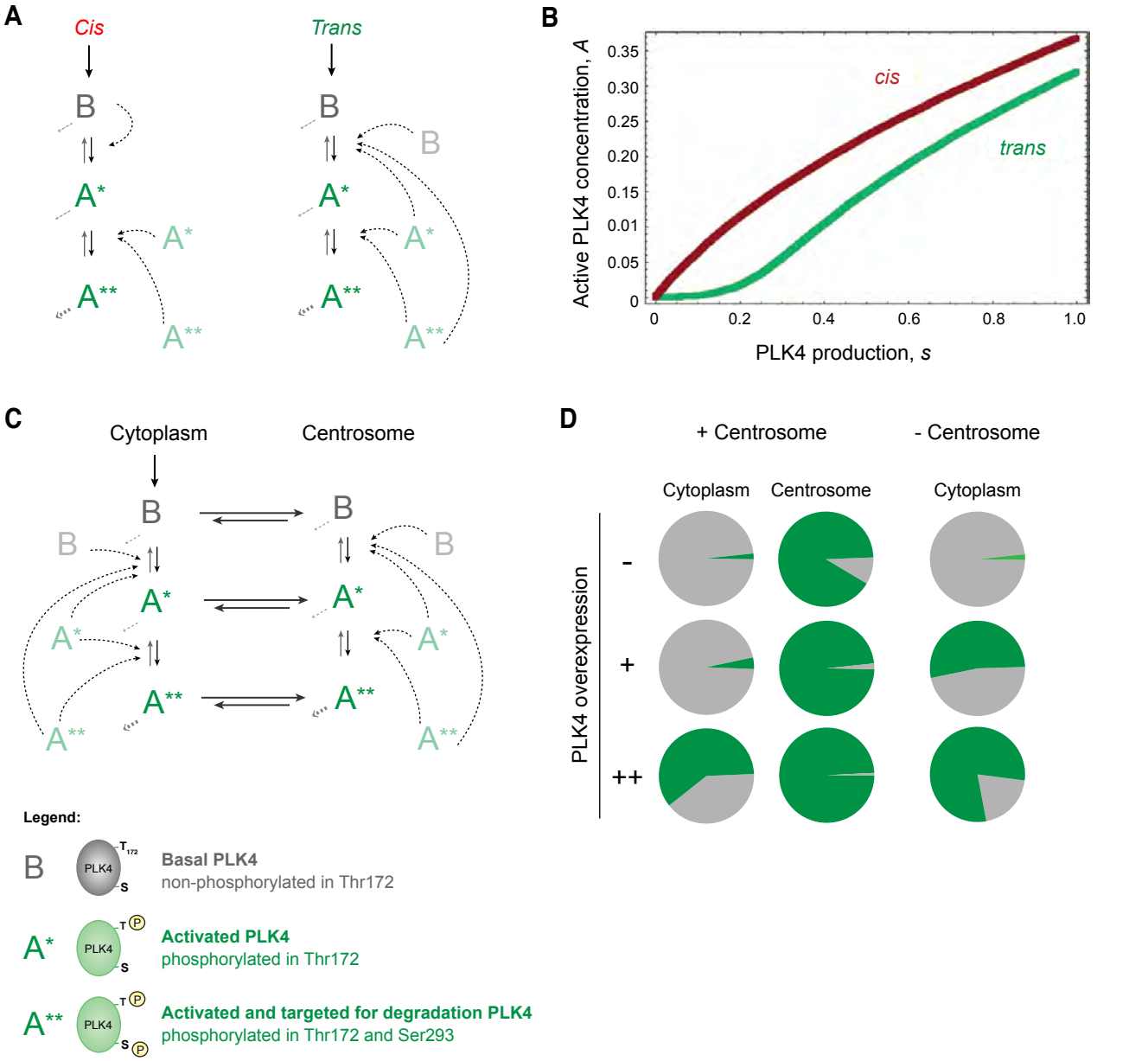
A
Cis
Trans
B
A*
A**
B
Active PLK4 concentration, A
0.35
0.30
0.25
0.20
0.15
0.01
0.05
0
cis
trans
0
0.2
0.4
0.6
0.8
1.0
PLK4 production, s
C
Cytoplasm
Centrosome
Legend:
Basal PLK4
non-phosphorylated in Thr172
Activated PLK4
phosphorylated in Thr172
Activated and targeted for degradation PLK4
phosphorylated in Thr172 and Ser293
D
+ Centrosome
- Centrosome
Cytoplasm
Centrosome
Cytoplasm
PLK4 overexpression
-
+
++

Figure 4

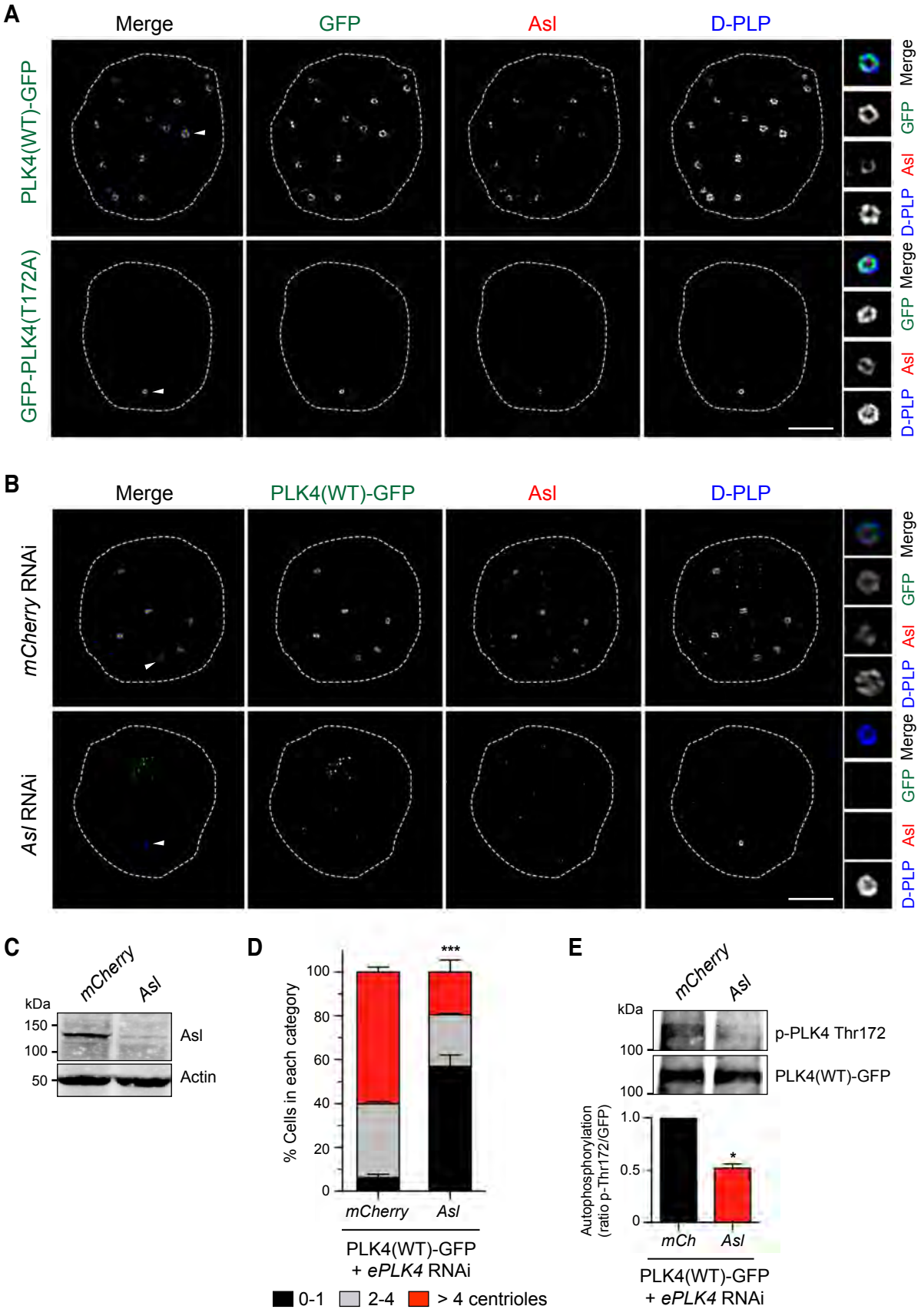
A
Merge
GFP
Asl
D-PLP
PLK4(WT)-GFP
GFP-PLK4(T172A)
B
Merge
PLK4(WT)-GFP
Asl
D-PLP
mCherry RNAi
Asl RNAi
C
mCherry
Asl
kDa
150
100
50
Asl
Actin
D
% Cells in each category
100
80
60
40
20
0
***
mCherry
Asl
PLK4(WT)-GFP
+ ePLK4 RNAi
0-1
2-4
> 4 centrioles
E
mCherry
Asl
kDa
100
p-PLK4 Thr172
PLK4(WT)-GFP
Autophosphorylation
(ratio p-Thr172/GFP)
1.0
0.5
0
*
mCh
Asl
PLK4(WT)-GFP
+ ePLK4 RNAi

Figure 5

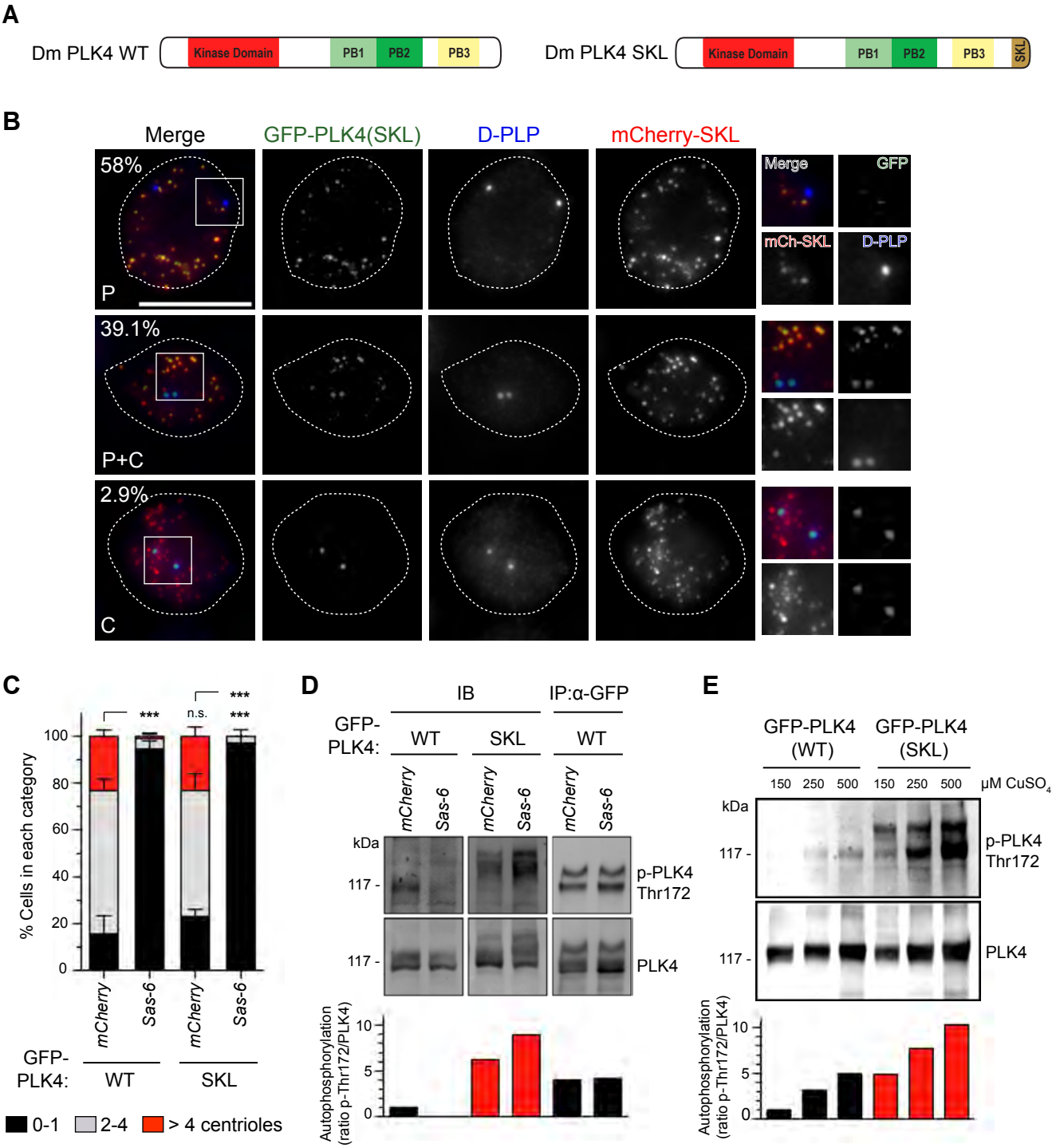
A
Dm PLK4 WT
Kinase Domain
PB1
PB2
PB3
Dm PLK4 SKL
Kinase Domain
PB1
PB2
PB3
SKL
B
Merge
GFP-PLK4(SKL)
D-PLP
mCherry-SKL
58%
P
39.1%
P+C
2.9%
C
Merge
GFP
mCh-SKL
D-PLP
C
% Cells in each category
100
80
60
40
20
0
***
n.s.
***
***
mCherry
Sas-6
mCherry
Sas-6
GFP-PLK4:
WT
SKL
0-1
2-4
> 4 centrioles
D
IB
IP:α-GFP
GFP-PLK4:
WT
SKL
WT
mCherry
Sas-6
mCherry
Sas-6
mCherry
Sas-6
kDa
117 -
p-PLK4 Thr172
117 -
PLK4
Autophosphorylation (ratio p-Thr172/PLK4)
10
5
0
E
GFP-PLK4 (WT)
GFP-PLK4 (SKL)
150
250
500
150
250
500
μM CuSO4
kDa
117 -
p-PLK4 Thr172
117 -
PLK4
Autophosphorylation (ratio p-Thr172/PLK4)
10
5
0

Figure 6

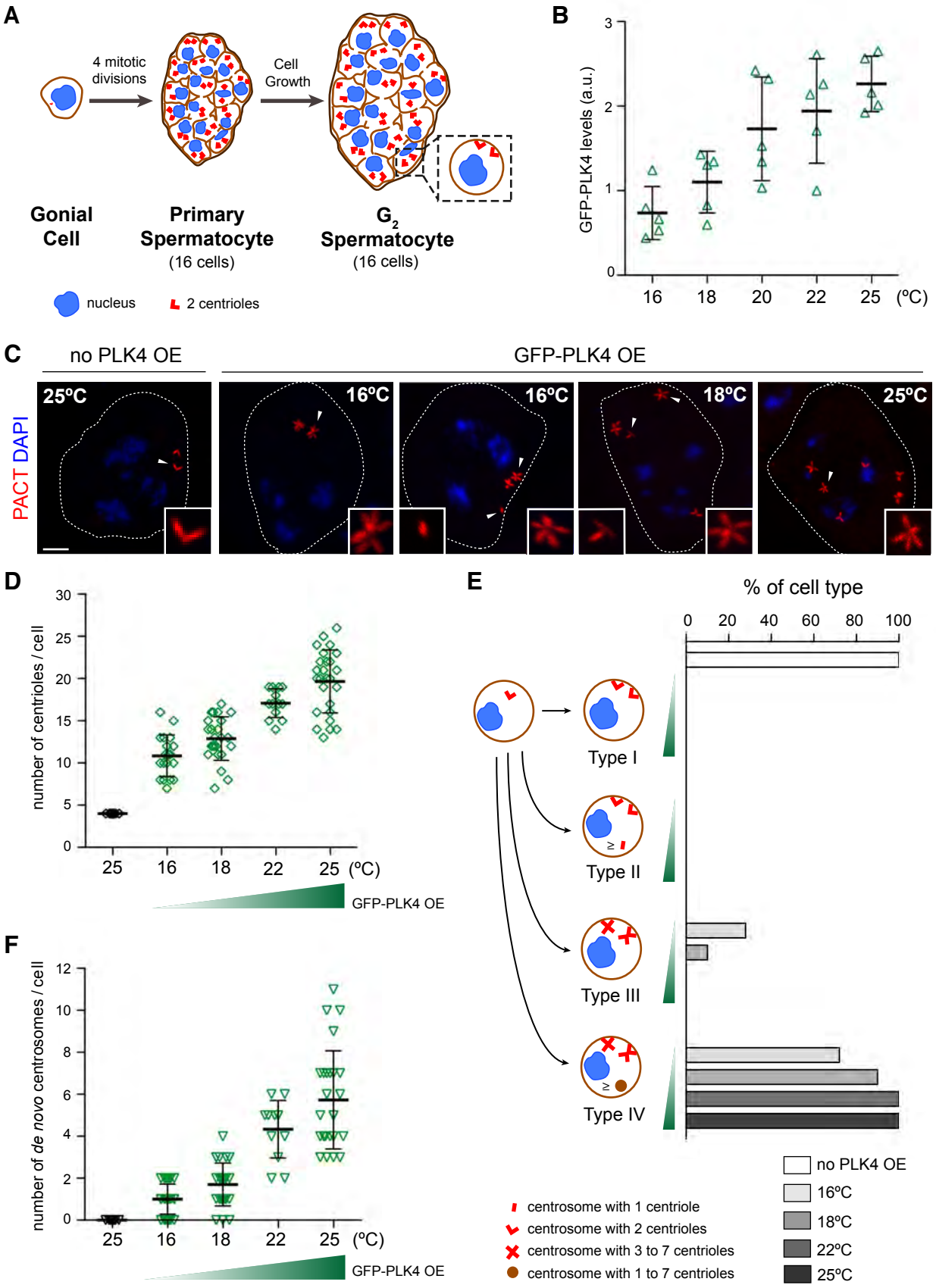
A
4 mitotic divisions
Cell Growth
Gonial Cell
Primary Spermatocyte
(16 cells)
G2 Spermatocyte
(16 cells)
nucleus
2 centrioles
B
GFP-PLK4 levels (a.u.)
0
1
2
3
16
18
20
22
25
(ºC)
C
no PLK4 OE
GFP-PLK4 OE
PACT DAPI
25ºC
16ºC
16ºC
18ºC
25ºC
D
number of centrioles / cell
0
5
10
15
20
25
30
25
16
18
22
25
(ºC)
GFP-PLK4 OE
E
% of cell type
0
20
40
60
80
100
Type I
Type II
Type III
Type IV
centrosome with 1 centriole
centrosome with 2 centrioles
centrosome with 3 to 7 centrioles
centrosome with 1 to 7 centrioles
no PLK4 OE
16ºC
18ºC
22ºC
25ºC
F
number of de novo centrosomes / cell
0
2
4
6
8
10
12
25
16
18
22
25
(ºC)
GFP-PLK4 OE

Figure 7

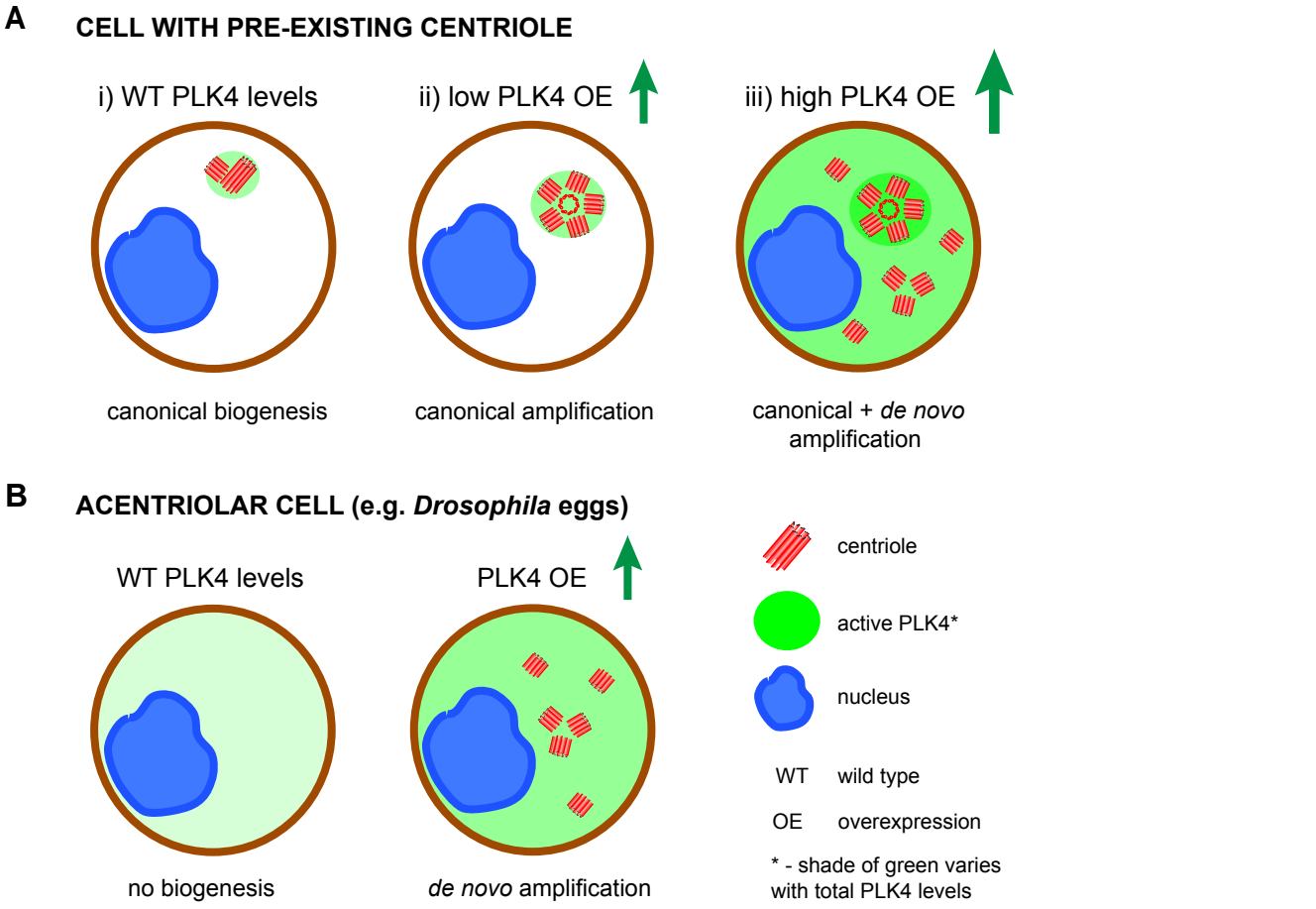
A
CELL WITH PRE-EXISTING CENTRIOLE
i) WT PLK4 levels
ii) low PLK4 OE
iii) high PLK4 OE
canonical biogenesis
canonical amplification
canonical + de novo amplification
B
ACENTRIOLAR CELL (e.g. Drosophila eggs)
WT PLK4 levels
PLK4 OE
no biogenesis
de novo amplification
centriole
active PLK4*
nucleus
WT wild type
OE overexpression
* - shade of green varies with total PLK4 levels

Supplementary information

Mathematical models of Polo-like-kinase 4 activity

We first considered a simple model of PLK4 activation in *cis* and in *trans* ignoring its localization in either the cytoplasm or the centrosome. The model features three forms of PLK4: a non-phosphorylated form, the active form phosphorylated in the T-loop, and the active form phosphorylated in both T-loop and degron. The dynamics of the concentrations of these forms, denoted respectively B, A^* and A^{**}, are described by the following differential equations:

$$\frac{dB}{dt} = s - dB - aBA - bB^2 - \alpha B + pA^* \quad (1)$$

$$\frac{dA^*}{dt} = aBA + bB^2 + \alpha B - cAA^* + pA^{**} - pA^* - dA^* \quad (2)$$

$$\frac{dA^{**}}{dt} = cAA^* - pA^{**} - d_c A^{**} \quad (3)$$

where the $A = A^* + A^{**}$ measures the sum of the two forms of active PLK4 kinases. The parameter s is the rate of synthesis of PLK4 (produced in the non-phosphorylated form); the right-hand side terms dB and dA^* represent the first order degron-independent degradation of non-phosphorylated and T-loop phosphorylated forms, respectively; $d_c A^{**}$ represents the first-order degron-dependent degradation of the double phosphorylated form; and the term cAA^* measures the *trans*-autophosphorylation of the active form in the degron. Finally, the terms aBA and bB^2 represent the phosphorylation of the non-phosphorylated PLK4 mediated by itself in *trans* and by the active form, respectively, while αB represents the *cis*-phosphorylation of the non-phosphorylated PLK4 form. This general formulation is convenient because by setting a to a positive value and α to zero, we define the scenario were activation acts only in *trans*-autophosphorylation, while by setting a to zero and α to a positive value defines the scenario of PLK4 *cis*-phosphorylation or PLK4 phosphorylation by another unspecified kinase, assumed to be at constant concentration.

We then extended the simple model formulated above to describe the exchange of the three forms of PLK4 and their partition between two compartments, the cytoplasm and the centrosome. The concentrations of each PLK4 form in either cytoplasm and centrosome is specific by the subindexes 1 or 2, respectively. The two-compartment model is described by the following 6 differential equations:

$$\frac{dB_1}{dt} = s - dB_1 - aB_1A_1 - bB_1^2 + pA_1^* + \rho r_2 B_2 - r_1 B_1 \quad (4)$$

$$\frac{dA_1^*}{dt} = aB_1A_1 + bB_1^2 - cA_1A_1^* + pA_1^{**} - pA_1^* - dA_1^* + \rho r_2 A_2^* - r_1 A_1^* \quad (5)$$

$$\frac{dA_1^{**}}{dt} = cA_1A_1^* - pA_1^{**} - d_cA_1^{**} + \rho r_2 A_2^{**} - r_1 A_1^{**} \quad (6)$$

$$\frac{dB_2}{dt} = -dB_2 - aB_2A_2 - bB_2^2 + pA_2^* - r_2 B_2 + r_1 B_1/\rho \quad (7)$$

$$\frac{dA_2^*}{dt} = aB_2A_2 + bB_2^2 - cA_2A_2^* + pA_2^{**} - pA_2^* - dA_2^* - r_2 A_2^* + r_1 A_1^*/\rho \quad (8)$$

$$\frac{dA_2^{**}}{dt} = cA_2A_2^* - pA_2^{**} - d_cA_2^{**} - r_2 A_2^{**} + r_1 A_1^{**}/\rho \quad (9)$$

where $A_i = A^*_i + A^{**}_i$ denote the total concentration of the two active (T-loop phosphorylated) PLK4 forms in the compartment indexed i. r_1 and r_2 are the rate constants of the fluxes from the cytoplasm to the centrosome and vice-versa, respectively. ρ denotes the volume ratio between cytoplasm and centrosome. The remaining parameters are defined as above. It is assumed that PLK4 is produce in non-phosphorylated form into the cytoplasm. The single and the two compartment model were analyzed by deriving the equilibrium solutions obtained when the left-hand side is set to zero and the system of equations solved in order of the 3 or 6 variables. Analytical and numeric equilibrium solutions were obtained using the software Mathematica 4.2 (Wolfram). The absolute quantity of the basal and active PLK4 forms in the two-compartment model were calculated as $\rho B_1 + B_2$ and $\rho A_1 + A_2$, respectively. Unless when otherwise indicated, the following set of reference parameters were used in all the figures of this article: s = 0.1, a = 40, b = 2, α = 40, c = 5, p = 10, d = 1, d_c = 40, ρ = 2000, r_1 = 5 and r_2 = 1.

Supplementary Experimental Procedures

In vitro kinase assay

In vitro kinase assay was performed using similar amounts of immunoprecipitated GFP-PLK4(WT), GFP-PLK4(T172A) and GFP-PLK4(KD) that were transiently expressed individually in DMEL cells previously treated with dsRNA for endogenous *PLK4* (*ePLK4* RNAi). 50 µl of Dynabeads coupled to GFP antibody were used to immunoprecipitate each construct. The beads were divided in two: half was used for the radioactive kinase assay and the other half to probe the total level of immunoprecipitated kinase by western blot. The radioactive *in vitro* kinase assay was performed with different GFP-PLK4 constructs in presence of 2 µg of MBP (Myelin Basic Protein, Santa Cruz) and 1 µCi of ATPγP^{32}. The mixtures were incubated 30 min at 18°C in the phosphorylation buffer (25 mM Tris pH7.5, 10 mM $MgCl_2$, 1 mM DTT). Kinase reactions were stopped and analyzed by SDS-PAGE.

Non-radioactive *in vitro* kinase assays

For non-radioactive kinase assays, 500 ng of recombinant His-MBP (Maltose Binding Protein)-PLK4 (pre-activated or not with regular ATP 1mM for 20 min) were diluted in the phosphorylation buffer in presence of 2 mM ATPγS (Abcam) and 5 µg MBP (Myelin Basic Protein) for 1 min at 18°C. The reactions were stopped with 80 mM EDTA and incubated for 2 hours with 1 mM 4-Nitrobenzyl mesylate (PNBM, Abcam) at RT to alkylate the thiophosphorylation site on the substrate. The kinase reaction was stopped and analysed by immunoblot using anti thiophosphate-ester (clone 51-8, Abcam) that recognises the phosphorylated MBP (Myelin Basic Protein).

In vitro auto-phosphorylation of PLK4

For *in vitro* autophosphorylation assays, His-MBP (Maltose Binding Protein)-PLK4(WT) was incubated for 10 min at 18ºC in 50 mM Tris-HCl pH 7.5 buffer

containing 1 mM ATP and 1 mM $MgCl_2$. Time points were taken every 2.5 min for testing autophosphorylation over the course of the experiment.

Supplementary Figure Legends

Figure S1 (related to Figure1) A) PLK4 Thr172 is required for PLK4 kinase activity. Following expression in DMEL cells depleted of endogenous *PLK4* (*ePLK4* RNAi), pMT-GFP-PLK4(WT), GFP-PLK4(T172A) and GFP-PLK4(KD) were immunoprecipitated with antibodies against GFP and used for kinase assays with MBP (Myelin Basic Protein) as a substrate. Autoradiograph (γP^{32}) for the MBP is shown. The amount of immunoprecipitated kinase was analyzed by western blot with antibodies against GFP. Coomassie stained gel shows the total MBP present as a substrate. Quantification of levels of MBP phosphorylation is shown. The values were normalized to the WT kinase. Data are the average of 3 experiments ± SEM (** $p<0.01$, *** $p<0.0001$ t-test). **B) T172A mutant is more stable than WT PLK4.** Expression of pMT-GFP-PLK4(WT), GFP-PLK4(T172A) and GFP-PLK4(KD) after depletion of endogenous PLK4 (*ePLK4* RNAi) in DMEL cells. Cell extracts were prepared and analyzed by western blot with antibodies against GFP and actin. Equal amounts of each extract were loaded. Actin was used as a loading control. Similar results were observed using the constructs from Figure 1C-D (i.e. Myc tagging) (not shown).

Figure S2 (related to Figure 2) A) p-PLK4 Thr172 is a phospho-specifc antibody raised against PLK4 Thr172 residue. DMEL cells expressing pMT-GFP-PLK4 were lysed and treated with lambda phosphatase (λ-ppase), λppase plus phosphatase inhibitors (PI) or PI alone. Upon PI treatment, the p-PLK4 Thr172 antibody recognizes a single western blot band corresponding to GFP-PLK4 phosphorylated at the Thr172. Note that this band is absent from the λ-ppase treated sample. **B) PLK4 autophosphorylates the Thr172 residue *in vitro*.** Autophosphorylation of

purified dephosphorylated His-MBP (Maltose Binding Protein)-PLK4(WT) followed for 10 minutes (min) after addition of ATP. Samples were taken at the indicated time points and probed by western blot with p-PLK4 Thr172 and His antibodies. Note that a very faint signal can be seen as soon as ATP is added (0 min). Quantification of the ratio of His-MBP-PLK4 phosphorylated at Thr172 to the total amount of PLK4 (His) is shown. The values were normalized to time point 10 min. Data are the average of 3 experiments ± SEM. Note that phosphorylation at Thr172 occurred very early and appears to increase non-linearly with time. **C) Pre-autophosphorylation of PLK4 activates this kinase.** Step 1: "Activation" – Dephosphorylated His-MBP (Maltose Binding Protein)-PLK4(WT) was either incubated with regular ATP (+) or not (-). Step 2: "Kinase assay" – PLK4 from Step 1 was used for kinase assays using MBP (Myelin Basic Protein) as a substrate in the presence of ATPγS. Samples were probed by western blot with antibodies against p-PLK4 Thr172 and His to detect phosphorylation on Thr172 and total levels of PLK4, respectively (after Step 1). MBP (Myelin Basic Protein) was equally loaded across lanes and its phosphorylation was analyzed by SDS-PAGE. Quantification of the ratio of MBP phosphorylation to the total amount of PLK4 (His) is shown. The ratios were normalized to the "non-active" kinase. A representative experiment is shown (out of 2). Note that because PLK4 activates itself extremely fast, PLK4 is also autoactivating in the presence of ATPγS in Step 2, thus becoming partly active during the kinase assay. Therefore, even this "non-activated" kinase shows some ability to phosphorylate the substrate. Nevertheless, we can observe a difference in catalytic activity when comparing: with and without "pre-activation".

Figure S3 (related to Figure 5) A) PLK4 is more stable in the absence of centrosomes. Expression of pMT-GFP-PLK4(WT) and pMT-GFP-PLK4 (ND) (cannot be targeted for degradation, see Figure 2B) in DMEL cells after depletion of

SAS-6 (*SAS-6* RNAi) for 12 days to remove centrosomes (*mCherry* RNAi used as a negative control) and depletion of endogenous *PLK4* (*ePLK4* RNAi). Cell extracts were prepared and analyzed by western blot with antibodies against GFP and actin. Equal amounts of each extract were loaded. Actin was used as a loading control. A representative experiment is shown (out of 3). Note that PLK4(WT) is significantly stabilized in the absence of centrosomes. This large difference is likely to result from degradation since it was not observed with a non-degradable (ND) construct. Similar results were observed in the absence of *Asl* (not shown). **B) PLK4(SKL) does not co-localize with Ana2 outside the centrosome.** Representative images of immunostaining of DMEL cells expressing GFP-PLK4(SKL) after depletion of SAS-6 (*SAS-6* RNAi) (*mCherry* RNAi used as a negative control) for 12 days. D-PLP (in blue) and Ana2 (in red (Antibody from Dzhindzev et al, 2014)). Individual cells are outlined by dashed lines that represent the cell outline as judged by the D-PLP background signal. Scale bar, 10 μm. Enlargements of the indicated areas (squares) are shown. Arrows in enlargements (top panel) indicate GFP-PLK4(SKL) co-localizing with Ana2 at the centrosome (D-PLP). Note that GFP-PLK4(SKL), which we have shown to localize to the peroxisome and centrosome (Figure 5 in the main manuscript) only co-localizes with Ana2 at the centrosome, and not at the peroxisome. This suggests that in the absence of centrosomes, overexpressed PLK4 can autoactivate at the lumen of the peroxisome, where no Ana2/STIL is detected.

Figure S1 (related to Figure 1)

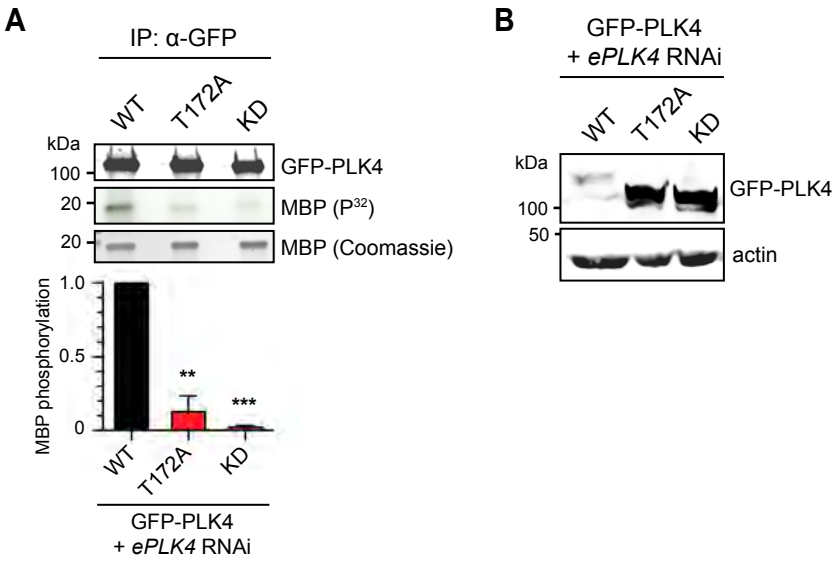

Supplemental Figure 2

Figure S2 (related to Figure 2)

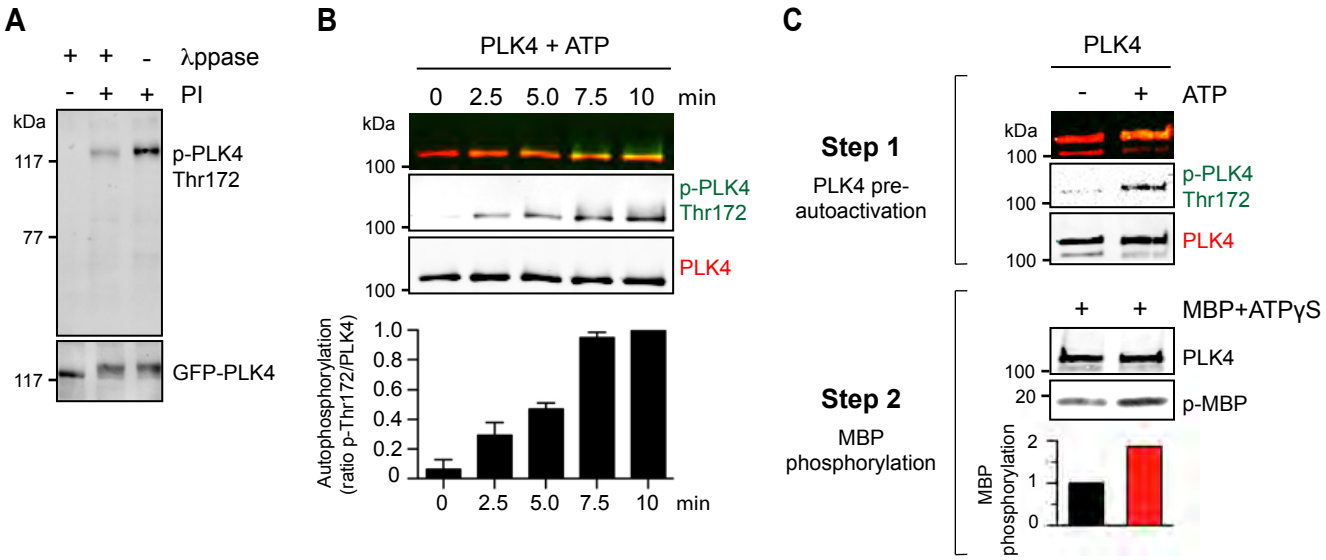

Figure S3 (related to Figure 5)